NASA

MEMORANDUM

ESTIMATION OF STATIC LONGITUDINAL STABILITY OF AIRCRAFT

CONFIGURATIONS AT HIGH MACH NUMBERS AND AT ANGLES

OF ATTACK BETWEEN 0° AND ±180°

By Duane W. Dugan

Ames Research Center
Moffett Field, Calif.

NATIONAL AERONAUTICS AND SPACE ADMINISTRATION

WASHINGTON

March 1959
Declassified February 6, 1962

NATIONAL AERONAUTICS AND SPACE ADMINISTRATION

MEMORANDUM 1-17-59A

ESTIMATION OF STATIC LONGITUDINAL STABILITY OF AIRCRAFT

CONFIGURATIONS AT HIGH MACH NUMBERS AND AT ANGLES

OF ATTACK BETWEEN 0° AND $\pm 180^\circ$

By Duane W. Dugan

SUMMARY

The possibility of obtaining useful estimates of the static longitudinal stability of aircraft flying at high supersonic Mach numbers at angles of attack between 0° and $\pm 180^\circ$ is explored. Existing theories, empirical formulas, and graphical procedures are employed to estimate the normal-force and pitching-moment characteristics of an example airplane configuration consisting of an ogive-cylinder body, trapezoidal wing, and cruciform trapezoidal tail. Existing wind-tunnel data for this configuration at a Mach number of 6.86 provide an evaluation of the estimates up to an angle of attack of 35°. Evaluation at higher angles of attack is afforded by data obtained from wind-tunnel tests made with the same configuration at angles of attack between 30° and 150° at five Mach numbers between 2.5 and 3.55. Over the ranges of Mach numbers and angles of attack investigated, predictions of normal force and center-of-pressure locations for the configuration considered agree well with those obtained experimentally, particularly at the higher Mach numbers.

INTRODUCTION

The design of an aircraft which is required to leave and re-enter the atmosphere poses a number of problems. For example, it is conceivable that re-entry into the atmosphere may be made advertently or inadvertently at any angle of attack between 0° and $\pm 180^\circ$. An angle of attack of the order of 30° or 40° may be desirable in order to decelerate rapidly without undue heating, or to develop sufficient lift to skip out of the atmosphere. Angles of attack between 0° and $\pm 180^\circ$ may also be encountered by air-to-air missiles launched by high-speed aircraft.

The purpose of this report is to explore the possibility of obtaining useful estimates of the static longitudinal stability of aircraft configurations at high supersonic Mach numbers and at angles of attack between 0° and $\pm 180^\circ$. To do this, existing theories, empirical formulas, and graphical procedures are employed to predict the normal-force and pitching-moment characteristics of a given airplane configuration over a range of angles of attack from 0° to $\pm 180^\circ$. The configuration for this study is shown in figure 1. Wind-tunnel data for this airplane up to an angle of attack of 35° at a Mach number of 6.86 are available for limited evaluation of the estimates. To obtain an indication of the accuracy of the predictions at higher angles of attack, a model of the same configuration is tested at angles of attack from 30° to 150° at each of five Mach numbers between 2.5 and 3.55.

It should be noted that the specific theories and procedures employed in this report are somewhat arbitrarily selected, and other choices are not precluded.

ANALYSIS

The aerodynamic characteristics of an aircraft configuration may be calculated by summing the aerodynamic characteristics of the isolated individual components and the effects due to the interference of one part upon the aerodynamic characteristics of the others. Thus the equations

$$C_N = C_{N_B} + C_{N_W} + C_{N_T} + \Delta C_{N_{B(W)}} + \Delta C_{N_{B(T)}} + \Delta C_{N_{W(B)}} + \Delta C_{N_{T(B)}} + \Delta C_{N_{T(W)}} + \Delta C_{N_{W(T)}}$$
(1)

$$C_m = C_{m_B} + C_{m_W} + C_{m_T} + \Delta C_{m_{B(W)}} + \Delta C_{m_{B(T)}} + \Delta C_{m_{W(B)}} + \Delta C_{m_{T(B)}} + \Delta C_{m_{T(W)}} + \Delta C_{m_{W(T)}}$$
(2)

provide a convenient framework for obtaining the static longitudinal stability of aircraft configurations consisting of various combinations of body, wing, and tail. The subscripts B, W, and T pertain to the body, exposed wing, and exposed tail, respectively; the terms $\Delta C_{N_{B(W)}}$, $\Delta C_{N_{W(B)}}$, etc., represent the interference effects of the exposed wing upon the body, of the body upon the exposed wing, etc. The notation used herein is given in appendix A.

The next several sections are devoted to developing procedures for estimating over a range of angles of attack from 0° to $\pm 180^\circ$ and for high Mach numbers the following: (1) normal forces and pitching moments of a fuselage consisting of a pointed or rounded nose section followed by a

cylindrical portion; (2) normal forces and pitching moments of an isolated wing (or tail); and (3) effects of interference of one part of a body-wing-tail configuration upon the normal forces and pitching moments of the others.

It should be clear that modification or extension of the procedures used here might be required in assessing the aerodynamic characteristics of configurations having features dissimilar to those of the one considered. Obviously, a number of the steps and calculations included in the present study would not be required in the case of a more simple configuration such as an all-wing configuration or a pointed body of revolution with stabilizing fins.

Forces and Moments on the Body

At high Mach numbers, the flow about a body of revolution can be approximated by the Newtonian concept which assumes that the individual particles comprising the fluid medium possess only translational velocities in the direction of flow and lose all their momentum in a direction normal to those surfaces on which they impinge. Based on this impact theory, the coefficient of pressure at any point on surfaces exposed directly to the flow is given by (see ref. 1)
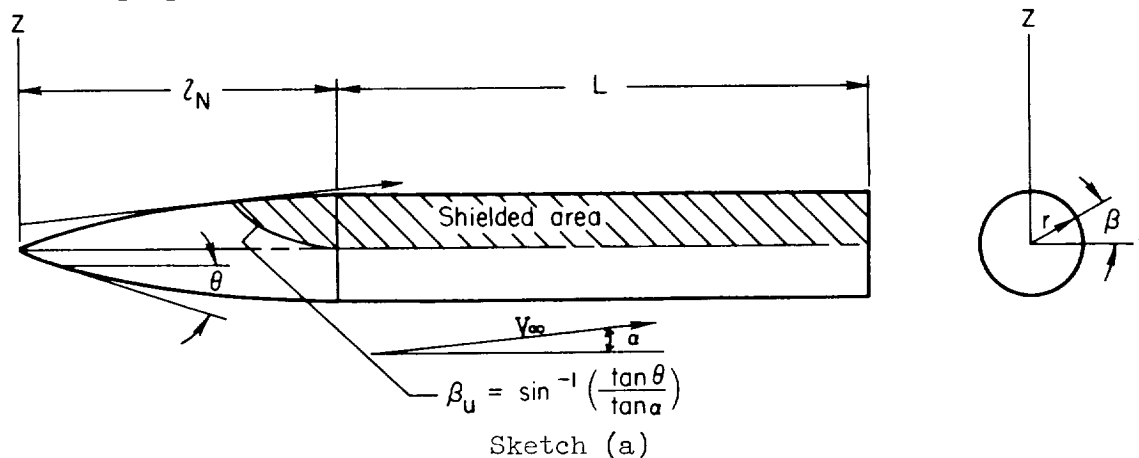
$$C_p = 2(\sin \theta \cos \alpha - \sin \alpha \cos \theta \sin \beta)^2 \tag{3}$$

where, as shown in sketch (a) below,

θ angle made by surface of body with body axis

α angle of attack of body axis

β polar angle of any point on body surface, measured from positive xy plane and positive for counterclockwise directions when viewed from rear

Sketch (a)

The value of the pressure coefficient on shielded surfaces C_{p_u} would be zero in the impact theory. Consideration of gasdynamics indicates that the value of C_{p_u} will vary between zero and $-2/\gamma M_\infty^2$ depending upon the free-stream Mach number, shape of the body, and angle of attack. According to reference 2, the lowest pressure in the flow about bodies is, from experimental evidence at subsonic and low supersonic Mach numbers, approximately 0.3 of the free-stream static pressure. In wind-tunnel tests (ref. 3) of a circular cylinder at angles of attack from $0°$ to $90°$ and at a Mach number of 6.86 the lowest pressure measured on the lee surfaces of the cylinder was approximately 0.34 of the free-stream static pressure. For a value of γ equal to 1.4, then, the largest negative value[1] of C_{p_u} appears to be of the order of $-1/M_\infty^2$. The mean value of the pressure coefficient over the shielded surfaces will thus be very small for large Mach numbers and can be considered as zero without significant effects on the calculated values of normal force and pitching moments.

For any portion of the fuselage shown in sketch (a), the normal force is given by

$$N = -2q_\infty \left[\int_{length} dx \left(\int_{-\pi/2}^{\beta_u} C_p r \sin \beta d\beta + \int_{\beta_u}^{\pi/2} C_{p_u} r \sin \beta d\beta \right) \right]$$

or, with C_p given by equation (3), and with C_{p_u} assumed zero,

$$\frac{dC_N}{dx} = \frac{2r}{S} \sin 2\alpha \cos^2\theta \left[\left(\beta_u + \frac{\pi}{2} \right) \tan \theta + \frac{1}{3} \cos \beta_u \left(\cot \alpha \, \tan^2\theta + 2 \tan \alpha \right) \right]$$

$$(4)$$

where S is a reference area. Likewise, the pitching moment, taken about the centroid of area of the base of the nose section for convenience, is given by

$$M = -2q_\infty \left\{ \int_{length} \left[\left(l_N - x \right) - r \tan \theta \right] dx \left(\int_{-\pi/2}^{\beta_u} C_p r \sin \beta d\beta + \int_{\beta_u}^{\pi/2} C_{p_u} r \sin \beta d\beta \right) \right\}$$

or

---

[1] Values of C_{p_u} negatively greater than $-1/M_\infty^2$ have been observed at supersonic speeds in tests of wings at moderate and large angles of attack; however, the magnitude of the coefficient is generally closer to $-1/M_\infty^2$ than to $-2/\gamma M_\infty^2$.

$$\frac{dC_m}{dx} = \frac{2r}{S\ell} \sin 2\alpha \, \cos^2\theta \left[\left(\ell_N - x\right) - r \, \tan \, \theta\right]\left[\left(\beta_u + \frac{\pi}{2}\right)\tan \, \theta \, + \right.$$

$$\left. \frac{1}{3} \cos \, \beta_u(\cot \, \alpha \, \tan^2\theta + 2 \, \tan \, \alpha)\right] \tag{5}$$

where ℓ is a reference length.

Equations (4) and (5) may be integrated analytically or numerically to give coefficients of normal force and pitching moment for any arbitrarily shaped body of revolution. Calculations for a conical nose are particularly simple, since θ = constant = θ_V, the semivertex angle of the cone, and r is a linear function of x. For positive angles of attack less than θ_V, $\beta_u = \pi/2$ and all surfaces are exposed to the flow, (i.e., C_p is defined for all values of β). For $\theta_V \leq \alpha \leq \pi - \theta_V$, portions of the cone are shielded from the flow, and $\beta_u = \sin^{-1}(\tan \, \theta_V/\tan \, \alpha)$. For $\pi - \theta_V \leq \alpha \leq \pi$, no surfaces of the cone are exposed to the flow and $\beta_u = -\pi/2$. In the above ranges of angles of attack the corresponding normal-force and pitching-moment coefficients based upon the area of the base and upon the length of the cone are

$$C_{N_{cone}} = \cos^2\theta_V \sin \, 2\alpha \, ; \quad 0 \leq \alpha \leq \theta_V \tag{6a}$$

$$C_{N_{cone}} = \frac{1}{\pi} \cos^2\theta_V \sin \, 2\alpha\left[\beta_u + \frac{\pi}{2} + \right.$$

$$\left. \frac{1}{3} \cos \, \beta_u(\cot \, \alpha \, \tan \, \theta_V + 2 \, \cot \, \theta_V \tan \, \alpha)\right] ; \quad \theta_V \leq \alpha \leq \pi - \theta_V \tag{6b}$$

$$C_{N_{cone}} = 0 \, ; \quad \pi - \theta_V \leq \alpha \leq \pi \tag{6c}$$

and

$$C_{m_{cone}} = \frac{1}{3} \, (1 - 2 \, \tan^2\theta_V)\cos^2\theta_V \sin \, 2\alpha \, ; \quad 0 \leq \alpha \leq \theta_V \tag{7a}$$

$$C_{m_{cone}} = \frac{1}{3\pi} \, (1 - 2 \, \tan^2\theta_V)\cos^2\theta_V \sin \, 2\alpha\left[\beta_u + \frac{\pi}{2} + \right.$$

$$\left. \frac{1}{3} \cos \, \beta_u(\cot \, \alpha \, \tan \, \theta_V + 2 \, \cot \, \theta_V \tan \, \alpha)\right] ; \quad \theta_V \leq \alpha \leq \pi - \theta_V \tag{7b}$$

$$C_{m_{cone}} = 0 \, ; \quad \pi - \theta_V \leq \alpha \leq \pi \tag{7c}$$

From the above results, the location of the center of pressure of the conical nose is independent of angle of attack; its distance from the vertex is given by

$$\frac{x_{cp}}{l_N} = \frac{2}{3} \left(1 + \tan^2\theta_V\right) \tag{8}$$

Calculations for other nose shapes are more involved since r, θ, and β_u are all functions of the lengthwise variable x. Inasmuch as the body-wing-tail configuration under consideration (fig. 1) has an ogival nose section, the integrations indicated in equations (4) and (5) are carried out for the circular-arc ogive with the following results:

$$C_{N_{ogive}} = \frac{2}{3} C^2 \sin 2\alpha \left\{ (1 - \eta^2)^2 - 2\sqrt{1 - \eta^2} + \frac{3}{2} \left(1 + \sec\alpha\right) - \right.$$
$$\left. \frac{8}{3\pi} \csc^2\alpha \, \sec\alpha\sqrt{1 - \eta^2} \left[(1 + k^2)E(k) - k'^2 K(k) \right] \right\}; \quad 0 \le \alpha \le \theta_V \tag{9a}$$

$$C_{N_{ogive}} = \frac{2}{3\pi} C^2 \sin 2\alpha \left\{ (1 - \eta^2)^2 \left(\frac{\pi}{2} + \sin^{-1} \frac{\eta}{\tan\alpha\sqrt{1 - \eta^2}} \right) - \right.$$
$$2\pi\sqrt{1 - \eta^2} + \frac{\eta}{3} \left[3(1 + \eta^2)\sin^2\alpha - \eta^2 + 4 \right] \csc\alpha \, \sec\alpha \, \cos\varphi + $$
$$3 \sec\alpha \, \sin^{-1} \frac{\eta}{\sin\alpha} + 3 \frac{\pi}{2} - \frac{8}{3} \csc^2\alpha \, \sec\alpha\sqrt{1 - \eta^2} \left[(1 + k^2)E(\varphi,k) - \right.$$
$$\left. \left. k'^2 F(\varphi,k) \right] \right\}; \quad \theta_V \le \alpha \le \pi - \theta_V \tag{9b}$$

$$C_{N_{ogive}} = \frac{2}{3} C^2 \sin 2\alpha \left\{ \frac{3}{2} \left(1 + \sec\alpha\right) - 2\sqrt{1 - \eta^2} - \right.$$
$$\left. \frac{8}{3\pi} \csc^2\alpha \, \sec\alpha\sqrt{1 - \eta^2} \left[(1 + k^2)E(k) - k'^2 K(k) \right] \right\}; \quad \pi - \theta_V \le \alpha \le \pi \tag{9c}$$

and

$$C_{m_{ogive}} = \frac{C^2}{15\eta} \sqrt{1-\eta^2} \sin 2\alpha \left\{ \left[\frac{40}{\pi} \alpha \csc^2\alpha - \frac{80}{3\pi} (3-\sin^2\alpha)\csc 2\alpha - \right.\right.$$

$$\left. 5\eta(3+2\eta^2) \right] \sqrt{1-\eta^2} - \frac{15}{4} \sin 2\alpha + 15\left(\sin^{-1}\eta - \frac{\alpha}{2}\right) +$$

$$\left. \frac{10}{\pi} (3+\sin^2\alpha)\csc 2\alpha - \frac{15}{\pi} \cos\alpha \cot^2\alpha \cosh^{-1}\sec\alpha + \frac{1}{56\pi} F_1 \right\} ;$$

$$0 \leq \alpha \leq \theta_v \tag{10a}$$

$$C_{m_{ogive}} = \frac{C^2}{9\pi\eta} \sqrt{1-\eta^2} \sin 2\alpha \left(\left\{ 24 \csc^2\alpha[\alpha - \tan^{-1}(\tan\alpha \cos\varphi)] - \right.\right.$$

$$16(3-\sin^2\alpha)\csc 2\alpha - 6\eta(3+\eta^2)\sin^{-1} \frac{\eta}{\tan\alpha\sqrt{1-\eta^2}} + \left[9+7\sin^2\alpha + \right.$$

$$\left. 2(3+\eta^2)(1-3\sin^2\alpha) \right] \csc\alpha \sec\alpha \cos\varphi - 3\eta(3+2\eta^2) \frac{\pi}{2} \right\} \sqrt{1-\eta^2} -$$

$$9 \cos\alpha \cot^2\alpha \left(\cosh^{-1}\sec\alpha - \cosh^{-1}\sec\alpha\sqrt{1-\eta^2} \right) +$$

$$6(3+\sin^2\alpha)\csc 2\alpha + 9 \frac{\pi}{2} \sin^{-1}\eta + \frac{3}{280} F_2 \right); \quad \theta_v \leq \alpha \leq \pi - \theta_v \tag{10b}$$

$$C_{m_{ogive}} = \frac{C^2}{9\pi\eta} \sqrt{1-\eta^2} \sin 2\alpha \left\{ 6(3+\sin^2\alpha)\csc 2\alpha - 9 \frac{\pi}{4} \sin 2\alpha + \frac{9\pi}{2} (\pi-\alpha) - \right.$$

$$9 \cos\alpha \cot^2\alpha \cosh^{-1}\sec\alpha - 8\left[2(3-\sin^2\alpha)\csc 2\alpha + \right.$$

$$\left. 3 \csc^2\alpha(\pi-\alpha) \right] \sqrt{1-\eta^2} + \frac{3}{280} F_3 \right\}; \quad \pi - \theta_v \leq \alpha \leq \pi \tag{10c}$$

In the above equations

$$\eta \qquad \frac{f_N}{C} = \frac{l_N}{R}$$

$$C \qquad \frac{R}{d}$$

R   radius of generating arc of ogive

f_N fineness ratio of nose $\dfrac{l_N}{d}$

k $\sin \alpha$

φ $\sin^{-1} \dfrac{\eta}{\sin \alpha}$

C_N, C_m $\dfrac{4N}{q\pi d^2}$, $\dfrac{4M}{q\pi d^2 l_N}$

and F_1, F_2, and F_3 are given in appendix B.

If $f_N = C = 1/2$, we have the hemispherical nose, and the above expressions for C_N and C_m become

$$C_{N_{hemisphere}} = \frac{1}{4} (\sin 2\alpha + 2 \sin \alpha) ; \quad 0 \le \alpha \le \pi$$

and

$$C_{m_{hemisphere}} = 0 ; \quad 0 \le \alpha \le \pi$$

In passing, it is interesting to compare the initial normal-force curve slopes of the cone and ogive for a given fineness ratio f_N. From the above results for the ogive,

$$\left(\frac{dC_N}{d\alpha}\right)_{\alpha=0} = \frac{4C^2}{3} (\cos^4\theta_v - 4 \cos \theta_v + 3)$$

$$= \frac{2}{3} \left[\frac{1 + 32f_N^4}{(1 + 4f_N^2)^2} \right]$$

and from equation (6a) for the cone,

$$\left(\frac{dC_N}{d\alpha}\right)_{\alpha=0} = 2 \cos^2\theta_v = \frac{8f_N^2}{(1 + 4f_N^2)}$$

The ratio of these slopes is

$$\frac{(C_{N\alpha})_{cone}}{(C_{N\alpha})_{ogive}} = \frac{12f_N^2(1 + 4f_N^2)}{1 + 8f_N^2 + 48f_N^4}$$

which is unity for $f_N = 1/2$ and ∞, is greater than unity for $1/2 < f_N < \infty$, and has a maximum value of only 1.06 when $f_N = 1/2\sqrt{1+\sqrt{2}} = 0.777$. For angles of attack near zero, therefore, the normal force of an ogive can be adequately obtained from the simple equation for that of the cone of equal fineness ratio. For fineness ratios of unity or larger, calculations show that the differences in C_N for the cone and ogive are negligible at angles of attack up to θ_V for the cone. At angles of attack somewhat less than θ_V of the cone, the curves of C_N versus α for the two nose shapes cross, so that at $\alpha = \theta_V$, C_N for the ogive exceeds that for the cone.

No explicit expression for the location of the center of pressure can be given for the ogive as in the case of the cone; computations have shown, however, that for small angles of attack the center of pressure of the ogive is nearer the vertex than that of the cone of equal fineness ratio and moves rearward with increasing angle of attack.

The contributions of the cylindrical portion of the fuselage to the normal force and pitching moment of the complete body when calculated from equations (4) and (5) are

$$C_{N_{cyl}} = \frac{16}{3\pi} \frac{L}{d} \sin^2\alpha; \qquad 0 \leq \alpha \leq \pi \qquad (11)$$

and

$$C_{m_{cyl}} = -\frac{8}{3\pi} \frac{L}{d} \frac{L}{l_N} \sin^2\alpha; \qquad 0 \leq \alpha \leq \pi \qquad (12)$$

where L is the length of the cylinder, and the coefficients are based on the same reference area and length as in the case of the nose section above.

Equations (11) and (12) do not include the effects of centrifugal forces in the flow about the cylinder, nor the effects of viscous forces (skin friction). These effects tend to cancel each other as shown by the results of tests on cylinders reported in reference 3. Equation (11) predicted normal forces in excellent agreement with the experimental force data at small to moderate angles of attack and overestimated such forces by only 5 percent near 90°. On the other hand, inclusion of the effects of centrifugal forces in the impact theory (ref. 1) gave values lower than those obtained experimentally by approximately 10 percent at the lower angles of attack and 5 percent near 90°.

Forces and Moments on Isolated Wing and Tail

Forces and moments on the isolated wing and horizontal tail are estimated over the range of angles of attack from $0°$ to $180°$ by a combination of two-dimensional shock-expansion theory (corrected for tip effects) and the Newtonian impact theory modified as discussed below.

For angles of attack not too near nor beyond the angle at which the bow wave of the wing or tail is detached, shock-expansion theory provides a good approximation to the lifting pressures in the absence of tip effects. The coefficient of normal force based on the exposed area of the wing is first calculated from two-dimensional shock-expansion theory for angles of attack up to that for shock-wave detachment. Next, if the reduced aspect ratio βA is so small that tip effects become appreciable, the two-dimensional results are multiplied by the ratio of the lift-curve slope of the finite wing to that of a wing of infinite span, both values being obtained from linearized supersonic theory. Values of lift-curve slopes for finite wings may be obtained readily from such sources as reference 4. The values of C_N thus obtained are plotted as a function of the angle of attack. Forces on a tail in the wake of a wing and vice versa are estimated subsequently in the section entitled "Interference Effects."

To the writer's knowledge, no methods exist for successfully predicting the lifting pressures on finite wings at angles of attack beyond that for shock detachment. The Newtonian impact theory, so useful in estimating normal forces on bodies of revolution for all angles of attack and even at comparatively low supersonic Mach numbers, is very inadequate in the case of planar surfaces. Even at very large Mach numbers the impact theory grossly underestimates the lifting pressures on an infinite flat plate at small to moderate angles of attack; on the other hand, the theory over-estimates the force on a plate placed normal to the free stream according to experimental evidence. In order to arrive at some logical basis for estimating the normal forces on a finite wing at angles of attack beyond which the shock-expansion method is inapplicable, the following approach is adopted.

First, the assumption is made that the variation of normal force on a flat surface at angles of attack in the immediate neighborhood of $90°$ is that given by the Newtonian concept; that is, the force varies as the second power of the sine of the angle of attack. Next, the impact theory is modified by replacing the factor 2 in the equation $C_N = 2 \sin^2\alpha$ by a factor in accord with experimental results for flat surfaces placed normal to the free supersonic stream. The third step is to fair an interpolating curve from the curve obtained above from considerations of shock-expansion theory (with any corrections necessary for tip effects) to the curve based on the modified Newtonian impact theory. This latter procedure will be discussed more in detail subsequently when an application to the wing of the example body-wing-tail configuration is made.

The choice of a factor to replace the factor 2 in the impact theory is made from the following considerations. Experimental measurements (refs. 5, 6, and 7, and unpublished data) of the pressure over the face of right circular cylinders with axes alined with the free supersonic stream indicate that the pressures remain nearly constant at the value given by gasdynamics for stagnation pressure p_s over approximately half the distance from the center of the face to the edges, and thereafter decrease to a value p_{so} corresponding to sonic velocity at the edge. The variation of the ratio of local pressures p to stagnation pressure p_s with fractional distance ξ from center to edge is shown in figure 2 for faces of cylinders of various diameters at several Mach numbers. Also shown in the figure is a plot of the equation

$$\frac{p}{p_s} = \frac{p_{so}}{p_s} + \left(1 - \frac{p_{so}}{p_s}\right)(1 - \xi^4)^{1/3}$$

which appears to fit the data within a few percent. The corresponding expression for the coefficient of pressure on the windward face is

$$C_{p_l} = \frac{2}{\gamma M_\infty^2}\left(\frac{p}{p_\infty} - 1\right) = C_{p_s}\left[\frac{C_{p_{so}}}{C_{p_s}} + \left(1 - \frac{C_{p_{so}}}{C_{p_s}}\right)(1 - \xi^4)^{1/3}\right]$$

where

ξ ratio of distance from geometric center to distance from center to edge

$C_{p_{so}}$ coefficient of pressure corresponding to sonic velocity

C_{p_s} coefficient of pressure corresponding to stagnation conditions

$\dfrac{C_{p_{so}}}{C_{p_s}}$ $\left(\dfrac{p_{so}}{p_s} - \dfrac{p_\infty}{p_s}\right)\left(1 - \dfrac{p_\infty}{p_s}\right)^{-1}$

$\dfrac{p_{so}}{p_s}$ 0.528 for $\gamma = 7/5$ in air

The coefficient of normal force for the windward face of the cylinder C_{N_l} based on the area of the face is then

$$C_{N_l} = \frac{1}{\pi}\int_0^{2\pi} d\theta \int_0^1 C_{p_l}\,\xi\,d\xi$$

$$C_{N_l} = C_{p_s}\left(0.842 + 0.158 \frac{C_{p_{so}}}{C_{p_s}}\right)$$

A comparison of the last equation with integrated experimental pressure distributions from several sources is presented in figure 3. Inasmuch as the distribution of pressure over a flat surface normal to the free supersonic stream is apparently determined primarily by the acceleration of the air from rest at the geometric center to sonic velocity at an edge, the equations given above for the flat face of circular plan form may be expected to serve as reasonable estimates for a variety of plan forms.

Now consider the pressures on the lee surfaces of flat plate shapes normal to the free stream. If viscosity is ignored, a Prandtl-Meyer expansion from sonic velocity would, of course, result in zero pressure over the lee surfaces, giving a pressure coefficient $C_{p_u} = -2/\gamma M^2$. As noted in an earlier section, there exists a limit pressure coefficient in air which has been found experimentally to have a value close to $-1/M_\infty^2$. The latter value is adopted here as the average pressure coefficient on the lee surfaces of flat shapes normal to supersonic flow. The total maximum normal-force coefficient is then

$$C_{N_{max}} = C_{p_s}\left(0.842 + 0.158 \frac{C_{p_{so}}}{C_{p_s}}\right) + \frac{1}{M_\infty^2} \tag{13}$$

Figure 4 shows a comparison of the above equation with experimental data obtained in ballistic firings and in wind-tunnel tests over a wide range of Mach numbers. These data are taken from references 8, 9, 10, and 11, and from unpublished results of tests in the Ames 10- by 14-inch wind tunnel. The data obtained in the Ames 10- by 14-inch wind-tunnel tests at nominal Mach numbers 3, 4, 5, and 6 indicate that the plan form of a flat wing at an angle of attack of $90°$ has but little effect on the total streamwise force. Pressure measurements made on the lee surfaces of the wings in the same tests substantiate the choice of $-1/M_\infty^2$ as the average value of C_{p_u}. From figure 4 it is concluded that the empirical equation derived here satisfactorily predicts normal-force coefficients for wings of various plan forms at $\alpha = 90°$ not only at large Mach numbers but at Mach numbers as low as 2. No reasons can be suggested here for the occurrence of a minimum value for C_N between Mach numbers 3 and 4 as indicated by the data; in any case, the discrepancies between predicted and experimental values of C_N are not so large, percentagewise, as to preclude the use of the empirical equation. The variation with Mach number of the stagnation pressure coefficient used in the equation is shown in figure 4 for comparison.

For the present purpose, the variation of the normal-force coefficient of an isolated wing or tail at angles of attack in the immediate

neighborhood of $90°$ will be estimated as $C_{N_{max}} \sin^2 \alpha$, with $C_{N_{max}}$ given by equation (13). There remains the problem of estimating the normal forces in the angle-of-attack range between angles of attack near shock detachment and those near $90°$. As noted earlier, graphical interpolation is used in the absence of theory or experimental data. Experimentally obtained variations of normal force with angle of attack up to and beyond shock detachment may serve as guides. For example, figure 5 presents the normal-force characteristics of a rectangular wing of aspect ratio 3 at angles of attack well beyond shock detachment for three different Mach numbers (ref. 12). Also shown in the figure are the modified impact values at $\alpha = 90°$ for each of the Mach numbers, together with interpolating curves. It is noted that at angles of attack well below those for shock detachment, the normal-force curves become increasingly concave with increasing Mach number as would be expected from predictions of two-dimensional shock-expansion theory; at angles of attack in the neighborhood of shock detachment, however, the curves are nearly linear, and become definitely convex at still larger angles. The above observations may also be made in the case of the normal-force characteristics of a triangular wing of aspect ratio 4 presented for two Mach numbers in figure 6 (ref. 13). The modified impact-theory values and interpolating curves are again drawn. Also shown in the figure is the variation of normal-force coefficient with angle of attack at $M_\infty = 6.86$ for the wing of the example configuration as calculated from two-dimensional shock-expansion theory. Although the profile of this wing has a rounded leading edge and a blunt trailing edge, for the purpose of calculation it was assumed that the profile was a symmetrical wedge-slab-wedge with sharp leading and trailing edges. The angle of attack at which shock detachment theoretically occurs is indicated in each case. The above angles were calculated according to the method presented in reference 14, which takes into account both the thickness of the profile and the leading-edge sweep of the wing. With the curves of the delta wing serving as qualitative guides, an interpolating curve for the example wing was drawn as shown. Values of normal-force coefficient for the isolated wing at angles of attack between $0°$ and $180°$ can then be obtained from the composite curve.

In the case of the tail of the example configuration, the wedge profile, although rounded, was assumed to be sharp-edged for purposes of calculation by means of two-dimensional shock-expansion theory. For rearward flight, because of the high Mach number, the shock wave was assumed to be effectively attached to the lower surface until the angle of flow deflection was equal to the angle calculated from two-dimensional shock-wave theory for shock detachment. The modified impact theory was based upon the angle made by the lower surface of the wedge with the free stream rather than the angle of attack.

To estimate the contributions of the isolated wing or horizontal tail to the pitching moment of the configuration, the center-of-pressure location is calculated by shock-expansion theory for angles of attack at

which the bow wave remains attached,[2] and thereafter extrapolated to the value given by impact theory at $\alpha = 90°$. In figure 7 the variation with angle of attack of the distance of the center of pressure from the leading edge of the mean aerodynamic chord of the exposed wing is plotted up to the angle at which the bow wave detaches. As in calculating normal forces above, the wing profile is assumed to be sharp-edged and symmetrical with respect to the midchord. Therefore, the center of pressure of the wing at $\alpha = 90°$ is at the centroid of area of the exposed wing, or at midchord of the mean aerodynamic chord. Since the tail of the example configuration has a wedge profile, the center of pressure is assumed to be at the centroid of area of the exposed tail at all angles of attack.

Interference Effects

In this section estimates are made for the effects upon normal force and pitching moments of (1) the wing and tail upon the body; (2) of the body upon the wing and tail; and (3) of the wing upon the tail (and vice versa) for angles of attack between $0°$ and $180°$. In most cases only first-order effects are considered; that is, the fact that the influence of the wing upon the body, for example, would affect the net influence of the body upon the wing which in turn would affect the influence of the wing upon the body, and so on, is neglected here since the extra labor involved would not be justified in the present method of estimation (cf. ref. 15). In assessing the influence of the horizontal tail upon the body in the case of the body-wing-tail configuration, however, the normal forces on the tail in the wake of the wing rather than in the free stream are used since no extra labor is involved and the effect upon the pitching moment of the configuration may be appreciable in some applications.

Sketch (b)

Body in presence of wing or tail.- In order to estimate the interference effects of the wing and tail upon the body, linearized supersonic theory is employed. The method of approximation outlined in reference 16 is adapted to the present problem. Sketch (b) above shows the essential

---

[2]These calculations can be used subsequently in determining the characteristics of the wake of the wing.

feature of the procedure in the case of a trapezoidal wing or tail of large span mounted on a cylindrical body. Note that for simplicity the cylindrical body is approximated by a plane surface of the same plan form; thus, the Mach cones which define the region of influence of the wing intersect the body in straight lines. The ratio of the normal force on the body due to the wing to that of the isolated exposed wing is given by (for $0^\circ \leq \alpha < 90^\circ$)

$$K_{B(W)} = \frac{N_{BW}}{N_W} = \frac{1}{N_W} \frac{8q\alpha m}{\pi\sqrt{\beta^2 m^2 - 1}} \left[\int_0^{d_1} dy \int_{\beta y}^{\beta y + c_r} \cos^{-1} \frac{x + m\beta^2 y}{\beta(y + mx)} dx + \int_{d_1}^{d_2} dy \int_{\beta y}^{h} \cos^{-1} \frac{x + m\beta^2 y}{\beta(y + mx)} dx \right]$$

(14)

which becomes

$$K_{B(W)} = \frac{8m\beta}{\pi\sqrt{\beta^2 m^2 - 1} \, (1 + \lambda_e) \frac{\beta d}{c_r} \left(\frac{2s}{d} - 1\right)\beta C_{N_\alpha}} \left\{ \frac{\sqrt{\beta^2 m^2 - 1}}{1 + m\beta} \left(\sqrt{2 \frac{h}{c_r} - 1} - 1\right) - \right.$$

$$\frac{1}{1 + m\beta} \left[(1 + m\beta) \frac{h}{c_r} - 1 \right]^2 \cos^{-1} \frac{(1 + m\beta) \frac{h}{c_r} - m\beta}{(1 + m\beta) \frac{h}{c_r} - 1} - \frac{m\beta}{1 + m\beta} \cos^{-1} \frac{1}{m\beta} +$$

$$\left(\frac{h}{c_r}\right)^2 \sqrt{\beta^2 m^2 - 1} \cos^{-1}\left(1 - \frac{c_r}{h}\right) + \frac{1}{m\beta} \left(\frac{\beta d_2}{c_r} + m\beta \frac{h}{c_r}\right)^2 \cos^{-1} \frac{\frac{h}{c_r} + m\beta \frac{\beta d_2}{c_r}}{m\beta \frac{h}{c_r} + \frac{\beta d_2}{c_r}} -$$

$$\left. \sqrt{\beta^2 m^2 - 1} \left[\left(\frac{h}{c_r}\right)^2 \cos^{-1} \frac{\beta d_2}{h} + \left(\frac{\beta d_2}{c_r}\right)^2 \frac{1}{m\beta} \cosh^{-1} \frac{h}{\beta d_2} \right] \right\}; \quad 0 \leq \alpha < \frac{\pi}{2}$$

(15)

where

$\beta \qquad \sqrt{M_\infty^2 - 1}$

$m \qquad$ cotangent of sweep angle of leading edge of wing

$h \qquad$ length of cylindrical portion of body from juncture of body and wing leading edge to base or $\beta d + c_r$, whichever is smaller

$c_r \qquad$ root chord of exposed wing

$\lambda_e \qquad$ taper ratio of exposed wing, $\frac{c_t}{c_r}$

s   semispan of wing-body combination

C_{N_α} normal-force curve slope of exposed isolated wing from linearized supersonic theory (see ref. 4)

Equation (15) is in its most general form. If $d_2 = h/\beta$ (the case shown in sketch (b)), the equation is somewhat simplified since the last two terms vanish. Likewise, if $h = \beta d + c_r$, then $d_1 = d_2 = d$, and the equation reduces to that given in reference 16.

The point at which this additional body normal force may be considered to act, $\bar{x}/c_r$ measured from the juncture of the leading edge of the wing and body, is found from

$$\frac{\bar{x}}{c_r} = \frac{M_{B(W)}}{N_{B(W)}c_r} = \frac{M_{B(W)}}{K_{B(W)}C_{N_\alpha}q\alpha d c_r^2(1+\lambda_e)\left(\frac{2s}{d} - 1\right)} \tag{16}$$

where $M_{B(W)}$, the moment of the induced normal force on the body about the juncture of the leading edge of the wing and the body, is calculated to be generally

$$M_{B(W)} = \frac{4q\alpha m c_r^3}{3\pi\beta}\left\{\left[\frac{2m\beta+5}{3(1+m\beta)^2} + \frac{\frac{h}{c_r}-1}{3(1+m\beta)}\right]\sqrt{2\frac{h}{c_r}-1} - \right.$$

$$\frac{1}{\sqrt{\beta^2 m^2 - 1}}\left[2(1+m\beta)\left(\frac{h}{c_r}\right)^3 - 3\left(\frac{h}{c_r}\right)^2 + \frac{1}{(1+m\beta)^2}\right]\cos^{-1}\frac{(1+m\beta)\frac{h}{c_r}-m\beta}{(1+m\beta)\frac{h}{c_r}-1} -$$

$$\frac{1}{\sqrt{\beta^2 m^2 - 1}}\left[1 - \frac{1}{(1+m\beta)^2}\right]\cos^{-1}\frac{1}{m\beta} + 2\left(\frac{h}{c_r}\right)^3\cos^{-1}\left(1 - \frac{c_r}{h}\right) - \frac{2m\beta+5}{3(1+m\beta)^2} +$$

$$\frac{1}{\sqrt{\beta^2 m^2 - 1}}\left[2m\beta\left(\frac{h}{c_r}\right)^3 + 3\left(\frac{h}{c_r}\right)^2\frac{\beta d_2}{c_r} - \frac{1}{m^2\beta^2}\left(\frac{\beta d_2}{c_r}\right)^3\right]\cos^{-1}\frac{\frac{h}{c_r}+m\beta\frac{\beta d_2}{c_r}}{m\beta\frac{h}{c_r}+\frac{\beta d_2}{c_r}} -$$

$$2\left(\frac{h}{c_r}\right)^3\cos^{-1}\frac{\beta d_2}{h} - \frac{1}{m\beta}\left(\frac{\beta d_2}{c_r}\right)^2\sqrt{\left(\frac{h}{c_r}\right)^2 - \left(\frac{\beta d_2}{c_r}\right)^2} +$$

$$\left. \frac{1}{m^2\beta^2}\left(\frac{\beta d_2}{c_r}\right)^3\cosh^{-1}\frac{h}{\beta d_2}\right\} ; \qquad 0 \le \alpha < \frac{\pi}{2} \tag{17}$$

and C_{N_α} is obtained as above from linearized supersonic theory.

If, as shown in sketch (b), $d_2 = h/\beta$, the last four terms in equation (17) vanish. If $h = \beta d + c_r$, then $d_1 = d_2 = d$, and equation (17) reduces to that given in reference 16.

The interference effects of the wing (or tail) upon the body in reversed flight ($90^\circ < \alpha \leq 180^\circ$) are found in the same manner as above with the proper values of m and h.

The interference normal forces and moments will be given by

$$\Delta C_{N_{B(W)}} = K_{B(W)} C_{N_W} \tag{18}$$

$$\Delta C_{N_{B(T)}} = K_{B(T)} C_{N_T} \tag{19}$$

$$\Delta C_{m_{B(W)}} = \Delta C_{N_{B(W)}} \left[\frac{x_{cg}}{l} - \frac{\bar{x}_{\Delta B(W)}}{l} \right] \tag{20}$$

and

$$\Delta C_{m_{B(T)}} = \Delta C_{N_{B(T)}} \left[\frac{x_{cg}}{l} - \frac{\bar{x}_{\Delta B(T)}}{l} \right] \tag{21}$$

where

C_{N_W} $\dfrac{N_W}{q_\infty S}$, coefficient of normal force of the exposed wing as estimated above from shock-expansion theory and modified impact theory

C_{N_T} $\dfrac{N_T}{q_\infty S}$, coefficient of normal force of the isolated tail in the case of wingless configurations as estimated above from shock-expansion theory and modified impact theory

$C_{N_{T(W)}}$ $\dfrac{N_{T(W)}}{q_\infty S}$, coefficient of normal force for the tail in the wake of the wing for $0^\circ < \alpha < 90^\circ$ in the case of body-wing-tail configurations as estimated below

S reference area

x_{cg} distance of moment reference from nose of fuselage

$\bar{x}_{\Delta B(W)}$ distance from nose of fuselage of the cp of the additional normal force on the body due to the wing

$\bar{x}_{\Delta B(T)}$ distance from nose of fuselage of the cp of the additional
normal force on the body due to the horizontal tail

l reference length

Obviously, the above method cannot be used for angles of attack for which the shock wave is detached from the wing or tail. At an angle of attack of 90°, impact theory implies no interference of the wing or tail upon the body; at finite high Mach numbers for which the detached bow wave at angles of attack near 90° clings closely to the wing or tail, the assumption that the above interference is negligibly small appears reasonable from consideration of gasdynamics. In order to arrive at some estimate of the additional forces and moments on the body due to the wing and tail over the ranges of angles of attack from 0° to 180°, resort to graphical interpolation is again made as shown in figures 8 through 13, where the procedure is applied to the example configuration at a Mach number of 6.86. In these figures, the curves for the aerodynamic characteristics of the body including wing or tail interference are faired smoothly into the corresponding curves of the body alone. The normal-force and pitching-moment coefficients of the body alone were calculated by adding the contributions of the ogival nose and of the cylindrical portion of the body obtained as discussed in the preceding section. The interference effects were obtained as indicated by equations (15) through (21), with $\beta C_{N_\alpha} = 4$ as for a two-dimensional supersonic wing. If it is assumed that the above interference is given closely by linearized supersonic theory for angles of attack not too near that for detachment of the bow wave and decreases gradually and monotonically toward zero as the angle of attack approaches 90°, then the difference between any two interpolating curves which might be employed to join the pairs of curves representing the aerodynamic characteristics of the body with and without interference is not likely to cause more than slight differences in final results for the complete configuration.

Wing and tail in presence of body.- As pointed out in reference 17, at very high supersonic speeds the normal force on a cylinder-wing combination (neglecting wing interference on the body) is approximately equal to the normal force of the wing alone if that portion of the wing covered by the cylinder is included. Here the covered portion of the wing is considered to be an extension of the root chord of the exposed wing through the cylinder in a diametral plane. The additional normal force on the exposed wing is, therefore, the difference between the normal force which would be carried by the portion of the wing covered by the body and that carried by the cylinder having a length equal to the root chord of the exposed wing.

From consideration of impact theory alone $(M_\infty \to \infty)$, the normal force on a flat plate wing having an area $c_{r_W}d$ is

$$N_{W_c} = 2q_\infty \sin^2\alpha\, c_{r_W} d$$

where

c_{r_W} root chord of exposed wing

d   diameter of cylindrical body

Likewise, the normal force of the cylindrical body of length c_{r_W} and diameter d is

$$N_{cyl} = \frac{4}{3} q_\infty \sin^2\alpha c_{r_W} d$$

The interference normal force on the exposed wing due to the presence of the body is then

$$\Delta N_{W(B)} = \frac{2}{3} q_\infty \sin^2\alpha c_{r_W} d$$

or

$$\Delta C_{N_{W(B)}} = \frac{1}{2} \frac{c_{r_W}}{L} C_{N_{cyl}} \tag{22}$$

where

$C_{N_{cyl}}$ $\frac{N_{cyl}}{q_\infty S_B}$, coefficient of normal force of cylindrical portion of body with length L as estimated in a preceding section

In the same way, the interference normal force on the tail is estimated as

$$\Delta C_{N_{T(B)}} = \frac{1}{2} \frac{c_{r_T}}{L} C_{N_{cyl}} \tag{23}$$

According to reference 17, these additional forces are concentrated in narrow regions adjacent to the wing-body and tail-body junctures. The pitching moments resulting from the interference normal forces on wing and tail due to the presence of the body can, therefore, be approximated by assuming that these forces act at the midchord position of the respective root chords of the exposed wing and tail.

The above estimates of interference effects are considered applicable in the present case over the entire range of angles of attack from 0° to 180°.

Tail in wake of wing.- In order to estimate the loads on a horizontal tail in the wake of the wing of a configui .tion flying at high supersonic speeds, the angle of flow, Mach number, and dynamic pressure of the wake must be determined. The procedure adopted here to obtain the above characteristics of the wake is described below as applied to the body-wing-tail configuration of figure 1.
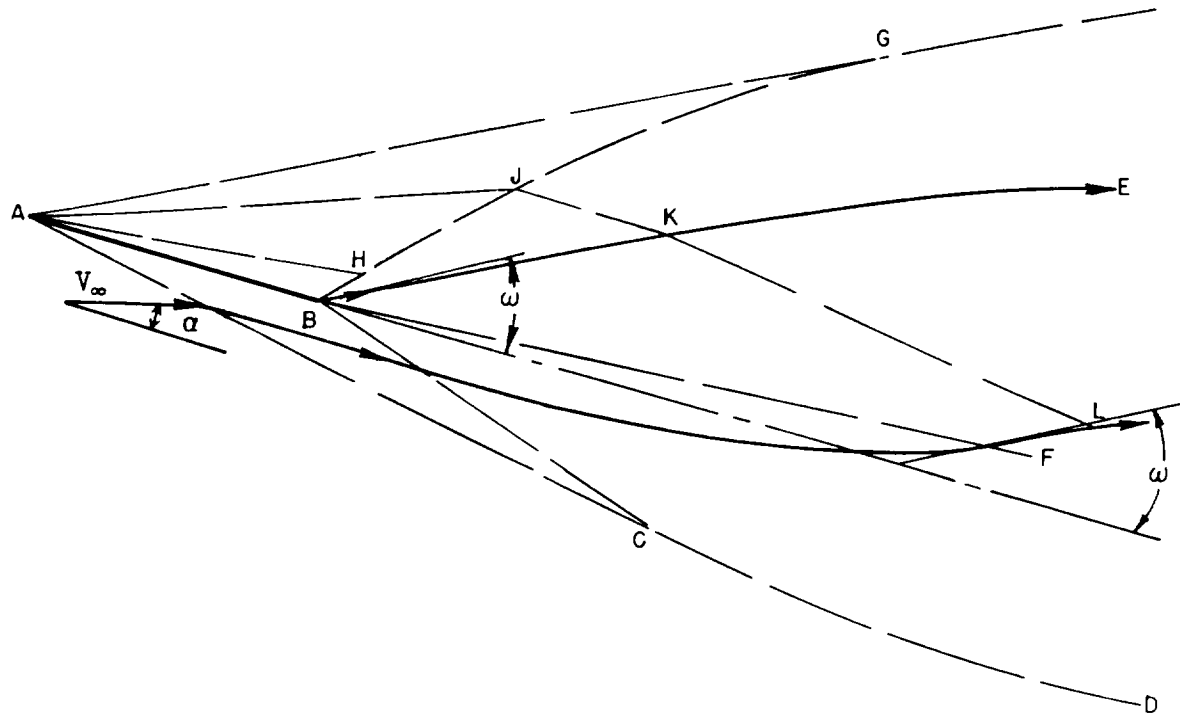
Sketch (c)

Sketch (c) shows the salient features of inviscid supersonic flow past a two-dimensional flat-plate wing of chord length AB at an angle of attack α. In the region ABC the fluid is compressed and turned to flow parallel to the lower surface; in the region CBF it next undergoes expansion and a turning back toward free-stream direction, and crosses the final expansion ray BF at an angle ω with respect to the chord plane. In general, the angle ω is larger than the angle of attack α. Beyond the point of intersection with the ray BF, the fluid eventually returns to free-stream direction. Above the wing, in the region ABG, the fluid is expanded and turned to flow parallel to the upper surface; as it crosses the terminal shock wave BHG, the fluid undergoes recompression and is turned toward the free-stream direction again, although its angle with respect to the wing chord as it crosses BHG is generally larger than α. Right at the trailing edge B, the fluid adjacent to the upper and lower surfaces of the wing leaves at the angle ω and follows the streamline BE. This streamline is often termed a "slip line" since there are discontinuities in velocity, Mach number, temperature, etc., (but not in pressure) across it. Reflections such as JK of the expansion waves between AH and AG from the shock wave BHG serve to return the streamline from the trailing edge to the free-stream direction at some point E as shown.

Although upwash occurs right at the trailing edge of the wing, the flow in the region GBC aft of the trailing edge may be characterized as either upwash or downwash depending upon the location in the region, upon

the free-steam Mach number, and upon the angle of attack of the wing. The other characteristics of the flow such as Mach number and dynamic pressure also depend upon the same parameters. The dynamic pressures of the wake decrease from comparatively high values in regions adjacent to BC to relatively low values above BF, while the Mach number of the wake increases with increasing distance from BC toward BE. Hence, as has been pointed out elsewhere (e.g., ref. 18), the effectiveness of a horizontal tail placed in that region of the wake above the chord plane of the wing will be generally less than that of one located below. In what follows, the horizontal tail is assumed to be located on or below the chord plane of the wing.

The pertinent characteristics of the flow behind the trailing edge of a two-dimensional wing at angles of attack less than that for shock detachment are estimated here on the basis of shock-expansion theory. For a given free-stream Mach number, the characteristics of the flow along any ray of the expansion fan CBF (sketch (d)) may be found conveniently by a
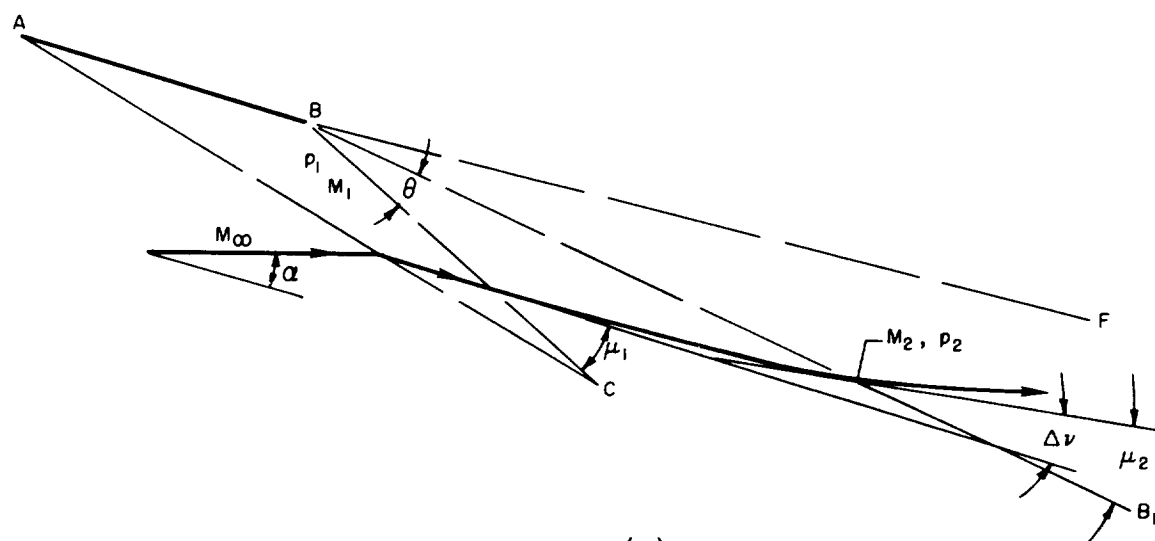
Sketch (d)

graphical procedure as follows: For a given angle of attack α, plot a curve of θ versus Δv with the latter as the independent variable from the relation

$$\theta = \Delta v + \mu_1 - \mu_2$$

where

$\Delta\nu \qquad \nu_2 - \nu_1$

ν_1,ν_2 angle through which air at $M = 1$ must turn in Prandtl-Meyer flow to accelerate to M_1,M_2

μ_1,μ_2 Mach angles, $\sin^{-1}\dfrac{1}{M_1}$, $\sin^{-1}\dfrac{1}{M_2}$

The value of $\Delta\nu$ for the flow across any ray is then read from the curve at the value of θ for the ray in question. Since M_1, p_1/p_∞, and ν_1 are known[3] for each angle of attack α, the value of ν_2 is determined and hence M_2 and p_2/p_1 may be found from Prandtl-Meyer relationships (most conveniently from tables of compressible flow such as are included in ref. 19). The ratio of the dynamic pressure of the flow at any point along a ray to that of the free-stream may be computed from

$$\frac{q_2}{q_\infty} = \left(\frac{M_2}{M_\infty}\right)^2\left(\frac{p_2}{p_1}\right)\left(\frac{p_1}{p_\infty}\right)$$

For a tail whose chord plane is alined with one of the rays in the expansion fan CBF, the direction, Mach number, and dynamic pressure will be constant along the chord. For other orientations of the tail, the above characteristics of the flow will vary along the chord of the tail; in such cases calculations for the forces at any spanwise station of the tail may be simplified somewhat without appreciable error by using the average of the flow characteristics at the leading and trailing edges, or by assuming that the flow calculated at the midchord is constant over the entire chord of the tail. For tails with zero dihedral angle, the spanwise distribution of pressure will be constant (excluding tip effects); for tails with positive or negative dihedral, the pressures will diminish or increase toward the tip, respectively, and graphical or numerical integration may be necessary to determine the total normal force on the tail.

At some Mach numbers and at small angles of attack, the tail may be outside the expansion fan CBF. In this case the flow approaching the tail will have completed its expansion and turning, and is then subject to recompression and a deflection in the opposite direction (toward free stream) through the influence of reflected disturbances from the flow over the upper surface of the wing such as the wave KL shown in sketch (c). However, for small angles of attack the above effects of the flow will not be large and in the few cases for which this situation exists the flow may be regarded as having the characteristics it had at the terminal expansion ray BF. The latter ray may be determined graphically from the stipulation that the common direction of the flow at the trailing edge coming from both lower and upper surfaces must be such that the recompression of the air passing over the upper surface and the expansion (in general) of the air from the lower surface result in the same value for the static pressure.

[3]These three quantities can be readily obtained from previous calculations for the center of pressure of the wing.

Certain aspects of the flow behind a wing at high supersonic speeds have been discussed in references 18 and 20. As noted in such references, the nature of the flow in the wake of a wing is determined to a considerable extent by the thickness of the wing; consequently, the direction, static pressure p_1, and Mach number M_1 used in the above procedure are calculated for the actual profile of the wing rather than for a flat plate.

The characteristics of the flow behind the wing of the configuration of figure 1 in the region of the tail were calculated according to the above procedure and are presented in figure 14. The profile of the wing was considered to be a wedge-slab-wedge for these calculations. The odd variation with angle of attack noted for the dynamic pressure in the wake is due to the combination of nonlinear relationships among the various parameters involved in shock-expansion theory. The final static pressure of a high-speed gas which is first subjected to a nonisentropic compression and then expanded isentropically depends in a nonlinear fashion upon both the extent of the compression and the amount of expansion. At angles of attack near that for shock detachment (40° in the present case) the increasing losses in total head across the oblique shock wave from the leading edge of the wing combined with increasing expansions in the wake were apparently sufficient to produce the downward trend in the variation of q_T noted in figure 14 at angles of attack near 40°.

Since the calculations for the normal force on the tail in the wake of the wing cannot extend beyond that angle of attack for which the shock wave detaches from the leading edge of either the wing or the tail, some means of estimating the force on the tail for the larger angles must be devised. At angles of attack near 90°, the wing will not appreciably affect the tail behind it. This fact suggests the use of graphical interpolation to approximate the force on the tail at large angles of attack as illustrated in figure 15. As indicated, the variation with angle of attack of C_N for the tail in the wake of the wing determined from shock-expansion theory is plotted up to the angle of attack for bow wave detachment. Also plotted in the figure is the same variation for the isolated tail in the free stream computed as explained in an earlier section from a combination of shock-expansion theory and modified impact theory. A third curve is then drawn to effect a transition from one computed curve to the other. The composite curve then represents the sum of the normal force of the tail and the interference normal force due to the wing and will be related to the term $C_{N_T} + \Delta C_{N_T(W)}$ of equation (1) in final calculations.

The contributions of the tail to the pitching moment of the body-wing-tail configuration will be based on the normal force of the tail in the wake of the wing and on the assumption that the center of pressure of the tail remains at the centroid of area of the exposed tail.

Wing in wake of tail.- The effects of the tail upon the aerodynamic characteristics of the wing (disregarding effects of the tail tips) may be estimated in much the same way as above. Inasmuch as the span of the tail is generally considerably less than that of the wing, the effect of the wake may extend over only a portion of the wing; consequently, the net effect on the normal force of the configuration may be comparatively small and the effect upon pitching moment is likely to be negligible for body-wing-tail configuration in which the wing is located close to the center of gravity.

The effect of the flow around the tail tips is confined within narrow Mach cones originating at the tail tips, so that at large Mach numbers the portion of the wing affected by such flow is likely to be comparatively small. In addition, the portion of the wing affected by the tail tip vortices will be divided into nearly equal regions of upwash and downwash, so that the net effect upon normal force and pitching moment of the complete configuration will generally be negligibly small.

Since for the present body-wing-tail configuration the effects of the wing upon the tail were not large (fig. 13), the effects of the tail upon the wing in reversed flight were judged to be too small to justify the calculations involved and were thus ignored.

COMPARISON BETWEEN PREDICTED AND EXPERIMENTAL
RESULTS FOR THE AIRPLANE CONFIGURATION

An evaluation of the foregoing estimates of normal-force and pitching-moment characteristics of the airplane configuration selected for this study is now made. Unfortunately, experimental data available at any given Mach number for comparison with the estimates do not extend over the complete range of angle of attack from $0°$ to $180°$. The airplane configuration considered here has been tested in the NASA Langley 11-inch blow-down wind tunnel at a Mach number of 6.86 up to angles of attack of $35°$. (Results up to $\alpha = 28°$ are published in ref. 21.) Figures 16, 17, and 18 give the comparison between predicted and experimental variations of normal force, pitching moment, and center-of-pressure location with angle of attack at $M_\infty = 6.86$, not only for the complete airplane but also for the body alone and the body-wing and body-tail combinations. As far as the experimental data permit comparison, the estimated results are in satisfactory agreement with the wind-tunnel tests in each case. A comparison between the results both with and without the inclusion of interference effects (fig. 19) indicates that inclusion of such effects should be made at the lower hypersonic Mach numbers such as 6.86.

To obtain an indication of the accuracy of the estimates at higher angles of attack the following procedure was followed. Available wind-tunnel facilities enabled testing of a model of the example configuration

over a range of nominal Mach numbers between 2.5 and 3.5. Accordingly, a model was constructed and tested at five Mach numbers in the given range at angles of attack between 30° and 150° in the test section of the Ames 8- by 7-foot Unitary Plan wind tunnel. The tests are described in appendix C of this report. The basic data obtained in the tests, normal-force coefficients and center-of-pressure locations, are presented in figures 20 and 21. The procedures described in the preceding sections were then applied to the complete configuration to give the estimated variation of normal-force coefficient and center-of-pressure location over a range of Mach numbers from 2.5 to 100. Predicted and experimental results (from faired curves of figs. 20 and 21) for a number of angles of attack between 30° and 150° are shown as a function of $1/M_\infty$ in figures 22 and 23. In general, the agreement between the estimated and experimental variation of normal force and center-of-pressure location with Mach number is good, not only qualitatively but quantitatively. However, at angles of attack near 90° (75° to 105°), the experimental variation of normal force differs somewhat from that predicted. Whereas a monotonic decrease of normal-force coefficient with Mach number is predicted at all angles of attack, the present data suggest that the coefficient may have a minimum value in the neighborhood of $M_\infty = 3.5$ for angles of attack between 75° and 105°. It may be recalled that, similarly, an apparent minimum in the normal-force coefficient of wings at $\alpha = 90^\circ$ was indicated between Mach numbers 3 and 4 by the data presented in figure 4. As a matter of interest, averaged experimental values of C_N from figure 4 were used for the wing and tail to calculate the normal-force coefficient of the complete example configuration at an angle of attack of 90°. The results are shown as the dotted curve in figure 22. Although the agreement between the calculated and experimental variation of normal force is generally improved by using experimental values for the wing and tail in this case, it is obvious that other factors are involved. Quantitatively, the discrepancies between the estimated and the present experimental values of C_N for the configuration at angles of attack between 75° and 105° are generally less than 5 percent except at angles near 100° where they are of the order of 10 percent. There is reason to believe, moreover, that the accuracy of the estimates of normal force for this configuration at angles of attack near 90° may be expected to improve with increasing Mach number beyond a Mach number of approximately 3.5.

Another phenomenon observed in the present tests which is not fully understood may be seen in figure 20. The abrupt decrease in normal force as the angle of attack increases from 90° to 100° is certainly not predicted as shown in figure 24 where the predicted variation of normal-force coefficient with angle of attack at a Mach number of 2.5 is compared with experimental data. The corresponding discrepancies between predicted and experimental pitching-moment curves are shown in figure 25. That the nature of the flow about the model changes as the attitude of the model changes from forward flight to rearward flight can be seen in a typical series of schlieren pictures taken during the present tests and presented

in figure 26. It is also possible that the shrouded sting and balance case attached to the lee side of the model in the tests may have contributed to disturbances in the flow over portions of the model in the subject angle-of-attack range more than anticipated. Whatever the causes, the data in figure 18 suggest that the distortion noted in the normal-force curves diminishes with increasing Mach number.

CONCLUDING REMARKS

Existing theories, empirical formulas, and graphical procedures have been employed in an attempt to predict normal-force and pitching-moment characteristics of a given airplane configuration at high supersonic Mach numbers and at angles of attack ranging from 0° to 180°. Availability of wind-tunnel data at a Mach number of 6.86 provided an evaluation of the predictions up to an angle of attack of 35°. To obtain an indication of the accuracy of the estimates at higher angles of attack, wind-tunnel tests of the same configuration were made at angles of attack between 30° and 150° over a range of Mach numbers from 2.5 to 3.55.

From a comparison between predicted and experimentally obtained values of normal-force coefficients and center-of-pressure locations over the range of Mach numbers and angles of attack investigated, it is concluded that for Mach numbers of the order of 5 and larger, close estimates of these characteristics are possible up to at least 150°. At Mach numbers between 2.5 and 3.55, the estimates agree well, in general, with the results of the wind-tunnel tests at angles of attack from 30° to 150°.

From the manner in which the estimates are obtained here at large angles of attack, application of the present procedures does not appear practical for Mach numbers much lower than 2.5, particularly for angles of attack larger than 90°.

In assessing aerodynamic characteristics of configurations having features dissimilar to those of the one considered, it should be clear that modification or extension of the procedures used in this report might be necessary. Obviously, a number of the steps and calculations included in the present study would not be required in the case of a more simple configuration such as an all-wing configuration or a pointed body of revolution with stabilizing fins.

Ames Research Center
    National Aeronautics and Space Administration
        Moffett Field, Calif., Oct. 17, 1958

APPENDIX A

NOTATION

$\bar{c}$	mean aerodynamic chord of entire wing or tail
c_r	root chord of exposed wing or tail
d	maximum diameter of nose section; diameter of fuselage
f	fineness ratio of body of revolution
k	modulus of elliptic integrals ($\sin \alpha$)
l	reference length
m	cotangent of angle of sweepback of leading edge of wing or tail
p	pressure at a given point on surface of body, wing, or tail
p_{∞}	static pressure in free stream
q	dynamic pressure, $\dfrac{\gamma M^2 p}{2}$
r	local radius of body of revolution
s	semispan of wing or tail of complete configuration
x,y,z	longitudinal, lateral, and vertical coordinates of a right-hand Cartesian coordinate system
C	caliber of ogive of revolution, $\dfrac{R}{d}$
C_m	coefficient of pitching moment, based on reference area S and on reference length l
C_N	coefficient of normal force, based on reference area S
C_p	coefficient of pressure, $\dfrac{p - p_{\infty}}{q_{\infty}}$
C_{p_s}	stagnation pressure coefficient, $\dfrac{p_s - p_{\infty}}{q_{\infty}}$

$C_{p_{so}}$ coefficient of pressure corresponding to sonic velocity

C_{p_u} coefficient of pressure in expansion regions of flow

$E(\varphi,k)$ incomplete elliptic integral of second kind

$E(k)$ complete elliptic integral of second kind

$F(\varphi,k)$ incomplete elliptic integral of first kind

$K(k)$ complete elliptic integral of first kind

L length of cylindrical portion of fuselage

$K_{B(W)}$ ratio of normal force on body due to presence of wing to normal force of exposed wing alone

M pitching moment; Mach number

N normal force

R radius of generating arc of circular-arc ogive

S reference area

V_∞ velocity of free stream

α angle of attack of body axis

β radial angle of a point on surface of body of revolution; cotangent of Mach angle

γ ratio of specific heats, $\dfrac{7}{5}$ for air

η ratio of length to radius of ogive, $\dfrac{l_N}{R}$

$\Delta C_{m_{B(W)}}$ additional pitching-moment coefficient of body due to presence of wing

$\Delta C_{m_{B(T)}}$ additional pitching-moment coefficient of body due to presence of tail

$\Delta C_{m_{T(B)}}$ additional pitching-moment coefficient of tail due to presence of body

$\Delta C_{m_{T(W)}}$ difference between pitching-moment coefficient of tail in wake of wing and that of isolated tail

$\Delta C_{m_{W(B)}}$ additional pitching-moment coefficient of wing due to presence of body

$\Delta C_{m_{W(T)}}$ difference between pitching-moment coefficient of wing in wake of tail and that of isolated wing

$\Delta C_{N_{B(W)}}$ additional normal-force coefficient of body due to presence of wing

$\Delta C_{N_{B(T)}}$ additional normal-force coefficient of body due to presence of tail

$\Delta C_{N_{T(B)}}$ additional normal-force coefficient of tail due to presence of body

$\Delta C_{N_{T(W)}}$ difference between normal-force coefficient of tail in wake of wing and that of isolated tail

$\Delta C_{N_{W(B)}}$ additional normal-force coefficient of wing due to presence of body

$\Delta C_{N_{W(T)}}$ difference between normal-force coefficient of wing in wake of tail and that of isolated wing

λ taper ratio of wing or tail

θ angle made by surface of body of revolution with body axis

θ_v semivertex angle of nose section

φ argument of elliptic integral, $\sin^{-1}\left(\dfrac{\eta}{\sin\alpha}\right)$

Subscripts

B   body or fuselage

c   cone

cg   moment reference

cp   center of pressure

cyl   cylinder

e   exposed wing or tail

l	lower surface of wing or body
N	nose section of body
T	horizontal tail
W	wing
∞	free-stream conditions

APPENDIX B

DERIVATIONS OF F_1, F_2, F_3

The expressions F_1, F_2, and F_3 of equation (10) in the text are the result of applying the method of integration in series to one intractable integral. The integral in question is

$$I = \int \sqrt{1 - t^2} \, \sin^{-1} \frac{t}{\tan \alpha \sqrt{1 - t^2}} \, dt$$

$$= \int \left(1 - \frac{t^2}{2} - \frac{t^4}{2 \cdot 4} - \frac{1 \cdot 3 t^6}{2 \cdot 4 \cdot 6} - \frac{1 \cdot 3 \cdot 5 t^8}{2 \cdot 4 \cdot 6 \cdot 8} - \ldots \right) \left(\sin^{-1} \frac{t}{\tan \alpha \sqrt{1 - t^2}} \, dt \right)$$

where $0 \leq t^2 \leq l_N^2 / R^2 \leq 1$. For most applications, only four terms of the series expansion above are necessary for good accuracy. Based upon the above approximate evaluation of the integral, the terms F_1, F_2, and F_3 are

$$F_1 = \frac{\pi}{2} \sin \alpha \left[1680 - (280 + 42 \sin^2\alpha + 15 \sin^4\alpha)\sin^2\alpha \right] -$$

$$1343 \, \alpha - \sin \alpha \cos \alpha \left[337 + (38 + 8 \sin^2\alpha)\sin^2\alpha \right]$$

$$F_2 = \eta \left[1680 - (280 + 42\eta^2 + 15\eta^4)\eta^2 \right] \sin^{-1} \frac{\eta}{\tan \alpha \sqrt{1 - \eta^2}} -$$

$$1343 \left(\alpha - \tan^{-1} \frac{\sqrt{\sin^2\alpha - \eta^2}}{\cos \alpha} \right) - \sin \alpha \cos \alpha \left[337 + (38 + 8 \sin^2\alpha)\sin^2\alpha \right] +$$

$$\cos \alpha \left[337 + (8 \sin^2\alpha + 38 + 4\eta^2)\sin^2\alpha + (3\eta^2 + 19)\eta^2 \right] \sqrt{\sin^2\alpha - \eta^2}$$

and

$$F_3 = \frac{\pi}{2} \sin \alpha \left[(280 + 42 \sin^2\alpha + 15 \sin^4\alpha)\sin^2\alpha - 1680 \right] +$$

$$1343(\pi - \alpha) - \sin \alpha \cos \alpha \left[337 + (38 + 8 \sin^2\alpha)\sin^2\alpha \right]$$

APPENDIX C

EXPERIMENTAL INVESTIGATION OF THE STATIC LONGITUDINAL
STABILITY OF THE AIRPLANE CONFIGURATION AT ANGLES
OF ATTACK BETWEEN 30° AND 150° AND AT MACH
NUMBERS BETWEEN 2.48 AND 3.55

As was stated in the text of this report, wind-tunnel data for the body-wing-tail configuration considered extend to only approximately 35° angle of attack at a Mach number of 6.86. To obtain an indication of the accuracy of the estimates at larger angles, the present investigation was conducted over a range of angle of attack from 30° to 150°. Inasmuch as the Mach number range of the available testing facility does not extend beyond 3.55, measurements were made at five different Mach numbers between 2.48 and 3.55 in order to determine the trend of normal force and center-of-pressure travel with Mach number.

Apparatus

The tests were conducted in the 8- by 7-foot test section of the Ames Unitary Plan wind tunnel. This wind tunnel is a continuous-flow, single-return type. The stagnation pressure can be held constant at values between 5 and 56 inches of mercury, and the Mach number can be varied during operation between nominal values of 2.4 and 3.5. The sting support has a range of ±14.65° in the pitch plane. Further details of this facility may be found in reference 22.

The model was a 4/3-scale replica of the airplane model tested in the Langley facilities. Figure 1 and table I give the essential features of the Langley model. For testing at angles of attack between 30° and 60°, the model was mounted from the downstream end on a 45° bent sting; for angles between 75° and 105°, it was supported by a straight sting attached dorsally at the midlength of the fuselage; for angles between 120° and 150°, the model was mounted as for the previous angle range except that a 45° bent sting was used in place of the straight sting. Each model sting was supported from a cylindrical balance case housing a six-component strain-gage-type balance. The balance itself was supported from the tunnel sting support. Both the balance case and model sting were shrouded to prevent aerodynamic forces other than those acting on the model from affecting the balance readings. A fouling indication system was provided to insure that the data would not be affected by mechanical interference between the shroud and model, sting or balance case.

In order to take into account any increments in the angle of attack of the model due to aerodynamic loads during the tests, a cathetometer was used to view the model through a window in the test section of the wind tunnel. By means of this instrument, the vertical distance between two points marked near either extremity of a midmeridian of the model body could be determined, and hence the actual angle of attack could be calculated.

Testing Procedure

For each of the three combinations of model and stings described above, readings of the fore-and-aft normal-force and of the axial-force balance gages were recorded by a strain-gage printer at each of several angular settings of the tunnel sting support for each of the five Mach numbers 2.48, 2.77, 3.07, 3.30, and 3.55. Several readings were repeated. The Reynolds number, based upon the mean aerodynamic chord of the model wing, varied from 240,000 to 510,000 during the tests.

Reduction of Data

The balance forces were resolved into the normal force on the model and into the position of the center of pressure. The model normal force was then reduced to standard NASA coefficient form based on the area of the entire wing of the model. The location of the center of pressure was referenced with respect to the nose of the model and made dimensionless in terms of the body length.

Precision of Results

Because of the manner in which the balance forces were resolved in each of the three model-sting-balance configurations, and because of the wide range in the magnitude of the forces on the model, the accuracy with which the values of C_N and x_{cp}/l_B could be obtained varied from one range of angles of attack to another. On the basis of the sensitivity of the instrumentation employed and upon the methods used to resolve the balance forces, as well as from consideration of the repeatability of results, the maximum errors in the measured quantities in the ranges of angles of attack noted are estimated to be

$$c_N \begin{cases} 30^\circ \leq \alpha \leq 60^\circ & \pm 0.010 \\ 75^\circ \leq \alpha \leq 105^\circ & \pm 0.012 \\ 120^\circ \leq \alpha \leq 150^\circ & \pm 0.024 \end{cases}$$

$$\frac{x_{cp}}{l_B} \begin{cases} 30^\circ \leq \alpha \leq 60^\circ & \pm 0.027 \\ 75^\circ \leq \alpha \leq 105^\circ & \pm 0.012 \\ 120^\circ \leq \alpha \leq 150^\circ & \pm 0.025 \end{cases}$$

$$\alpha \begin{cases} 30^\circ \leq \alpha \leq 60^\circ & \pm 0.15^\circ \\ 75^\circ \leq \alpha \leq 105^\circ & \pm 0.20^\circ \\ 120^\circ \leq \alpha \leq 150^\circ & \pm 0.15^\circ \end{cases}$$

It is not known just what effects the sting shroud had on the flow over the lee side of the model; however, it is believed such effects were negligible with regard to total normal forces and relatively small as far as the position of the center of pressure was concerned.

REFERENCES

1. Grimminger, G., Williams, E. P., and Young, G. B. W.: Lift on Inclined Bodies of Revolution in Hypersonic Flow. Jour. Aero. Sci., vol. 17, no. 11, Nov. 1950, pp. 675-690.

2. Mayer, John P.: A Limit Pressure Coefficient and an Estimation of Limit Forces on Airfoils at Supersonic Speeds. NACA RM L8F23, 1948.

3. Penland, Jim A.: Aerodynamic Characteristics of a Circular Cylinder at Mach Number 6.86 and Angles of Attack Up to 90°. NACA TN 3861, 1957.

4. Lapin, Ellis: Charts for the Computation of Lift and Drag of Finite Wings at Supersonic Speeds. Rep. No. SM-13480, Douglas Aircraft Co., Inc., Oct. 1949.

5. Boison, J. C., and Curtiss, H. A.: Preliminary Results of Spherical-Segment Blunt Body Pressure Surveys in the 20 Inch Supersonic Wind Tunnel at J. P. L. AVCO RAD Tech. Memo. 2-TM-57-77, 1957.

6. Stoney, William E., Jr., and Markley, J. Thomas: Heat-Transfer and Pressure Measurements on Flat-Faced Cylinders at a Mach Number of 2. NACA TN 4300, 1958.

7. Fraasa, Donald G.: An Experimental Investigation of Hypersonic Flow Over Blunt-Nosed Bodies at a Mach Number of 5.8. Thesis for Degree of Aeronautical Engineer, Cal. Inst. of Tech., 1957.

8. Walchner, O.: Systematic Wind-Tunnel Measurements on Missiles. NACA TM 1122, 1947.

9. Penland, Jim A., and Armstrong, William O.: Preliminary Aerodynamic Data Pertinent to Manned Satellite Re-entry Configurations. NACA RM L58E13a, 1958.

10. Long, J. E.: Supersonic Drag Coefficients of Circular Cylinders Up to Mach Number 8. NAVORD Rep. 4382, White Oak, Md., 1956. (Also available as Naval Ordnance Lab. Aeroballistic Res. Rep. 353)

11. Canning, Thomas N., and Sommer, Simon C.: Investigation of Boundary-Layer Transition on Flat-Faced Bodies of Revolution at High Supersonic Speeds. NACA RM A57C25, 1957.

12. Pitts, William C.: Force, Moment, and Pressure Distribution Characteristics of Rectangular Wings at High Angles of Attack and Supersonic Speeds. NACA RM A55K09, 1956.

13. Kaattari, George E.: Pressure Distributions on Triangular and Rectangular Wings to High Angles of Attack - Mach Numbers 2.46 and 3.36. NACA RM A54J12, 1955.

14. Bertram, Mitchel H., and McCauley, William D.: Investigation of the Aerodynamic Characteristics at High Supersonic Mach Numbers of a Family of Delta Wings Having Double-Wedge Sections With the Maximum Thickness at 0.18 Chord. NACA RM L54G28, 1954.

15. Lawrence, H. R., and Flax, A. H.: Wing-Body Interference at Subsonic and Supersonic Speeds - Survey and New Developments. Jour. Aero. Sci., vol. 21, no. 5, May 1954, pp. 289-324.

16. Pitts, William C., Nielsen, Jack N., and Kaattari, George E.: Lift and Center of Pressure of Wing-Body-Tail Combinations at Subsonic, Transonic, and Supersonic Speeds. NACA Rep. 1307, 1957.

17. Ivey, H. Reese, and Morrissette, Robert R.: An Approximate Determination of the Lift of Slender Cylindrical Bodies and Wing-Body Combinations at Very High Supersonic Speeds. NACA TN 1740, 1948.

18. Ulmann, Edward F., and Ridyard, Herbert W.: Flow-Field Effects on Static Stability and Control at High Supersonic Mach Numbers. NACA RM L55L19a, 1956.

19. Ames Research Staff: Equations, Tables, and Charts for Compressible Flow. NACA Rep. 1135, 1953.

20. Kahane, A., and Lees, Lester: The Flow at the Rear of a Two-Dimensional Supersonic Airfoil. Jour. Aero. Sci., vol. 15, no. 3, March 1948, pp. 167-170.

21. Penland, Jim A., Ridyard, Herbert W., and Fetterman, David E., Jr.: Lift, Drag, and Static Longitudinal Stability Data From an Exploratory Investigation at a Mach Number of 6.86 of an Airplane Configuration Having a Wing of Trapezoidal Plan Form. NACA RM L54L03b, 1955.

22. Manual for Users of the Unitary Plan Wind Tunnel Facilities of the National Advisory Committee for Aeronautics. NACA, Washington, 1956.

TABLE I.- GEOMETRIC CHARACTERISTICS OF LANGLEY MODEL (REF. 21)

Wing
  Area (including area submerged in fuselage), sq in. 6.240
  Area (exposed), sq in. 4.402
  Mean aerodynamic chord (entire wing), in. 1.713
  Mean aerodynamic chord (exposed wing), in. 1.456
  Span, in. 4.330
  Root chord (entire wing), in. 2.530
  Root chord (exposed wing), in. 2.133
  Tip chord, in. 0.354
  Aspect ratio (entire wing) 3.000
  Sweep of leading edge, deg 38.830
  Sweep of c/4 line, deg 29.000
  Incidence at fuselage center line, deg   0
  Dihedral, deg   0
  Geometric twist, deg   0
Horizontal and vertical tails
  Area (including area submerged in fuselage), sq in. 2.060
  Area (exposed), sq in. 1.204
  Span, in. 2.690
  Mean aerodynamic chord (entire tail), in. 0.853
  Mean aerodynamic chord (exposed tail), in. 0.571
  Root chord (entire tail), in. 1.214
  Root chord (exposed tail), in. 0.950
  Tip chord, in. 0.317
  Aspect ratio 3.520
  Sweep of leading edge, deg 22.63
  Dihedral, deg   0
Fuselage
  Length, in. 7.500
  Maximum diameter, in. 0.790
  Fineness ratio 9.500
  Base diameter, in. 0.790
  Distance from nose to moment reference, in. 3.950
  Maximum cross-sectional area, sq in. 0.490
  Ogive nose length, in. 2.290
  Ogive radius, in. 6.850
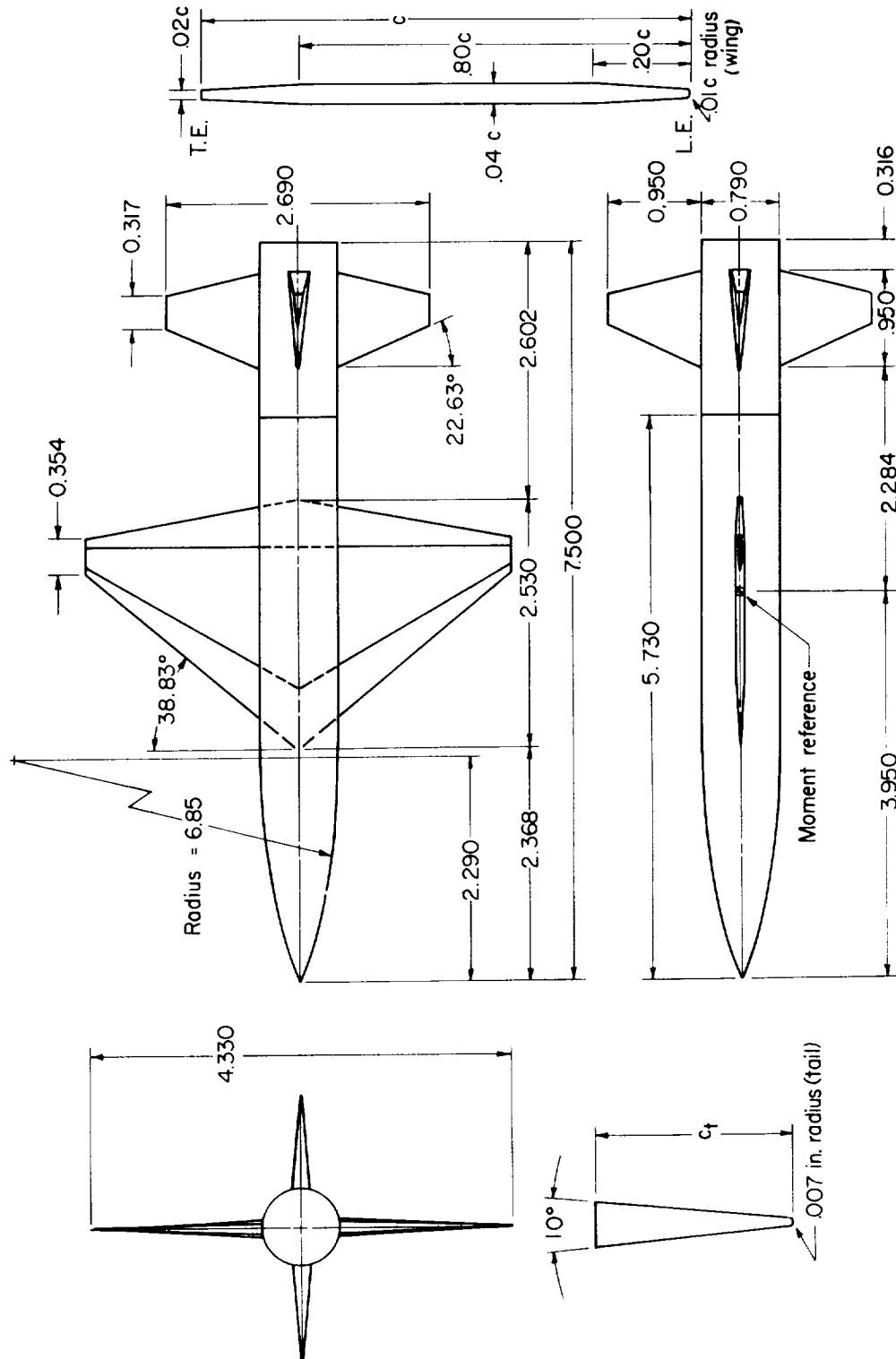
Figure 1.- Three-view sketch of example airplane configuration tested in Langley 11-inch hypersonic wind tunnel (ref. 21); all dimensions in inches.
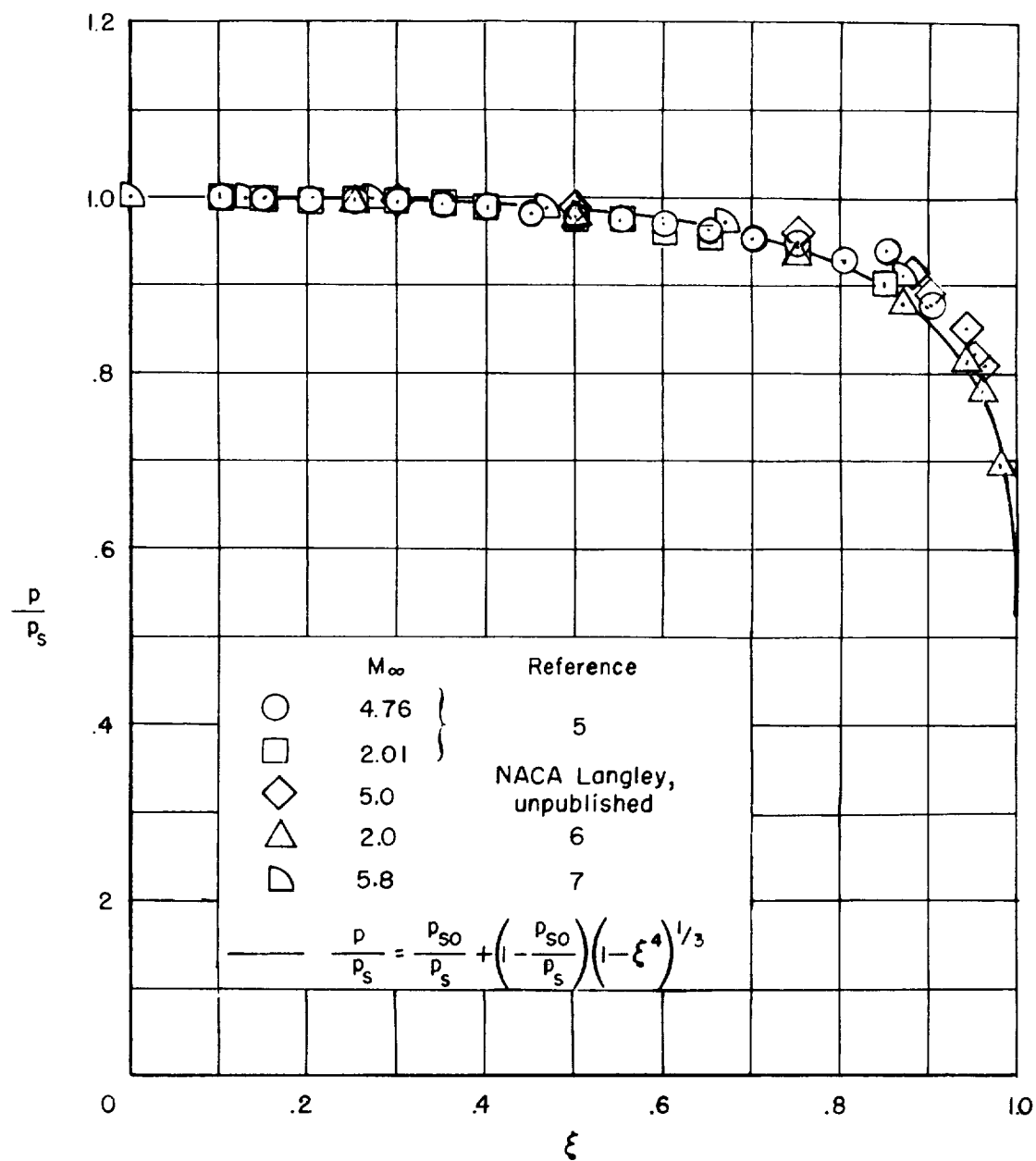
Figure 2.- Pressure distribution over flat faces of circular cylinders
with axes parallel to free stream.
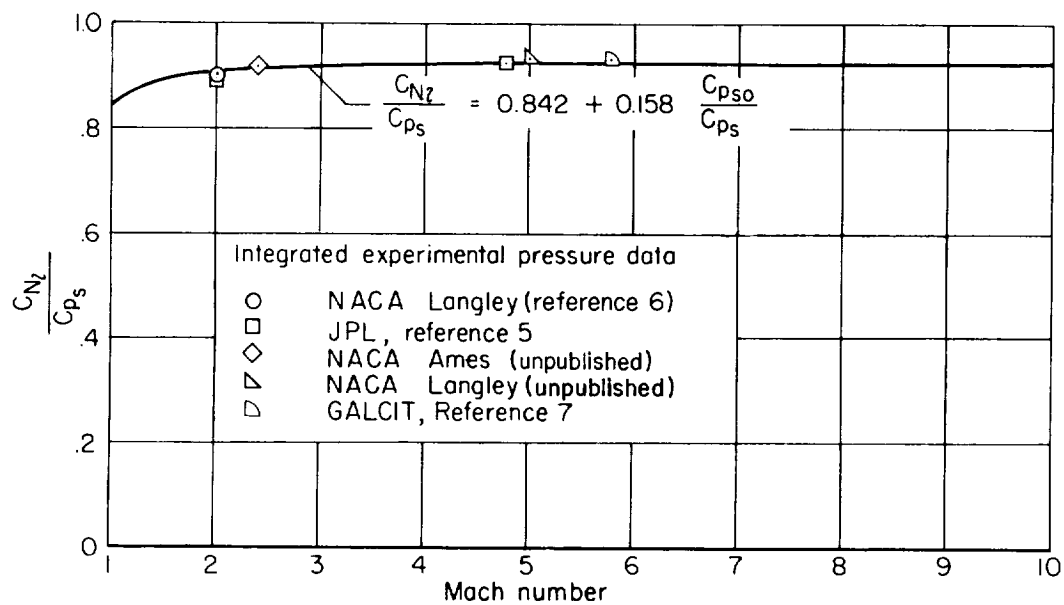
Figure 3.- Variation with Mach number of normal force due to pressures on windward faces of cylinders with axes parallel to free stream.
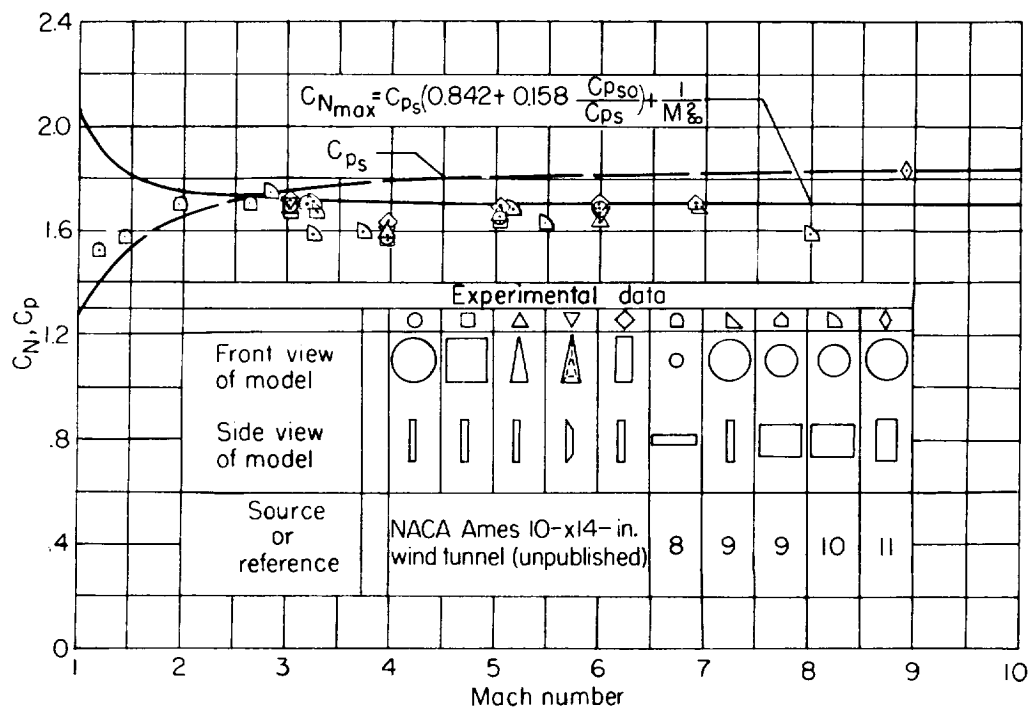
Figure 4.- Variation with Mach number of total streamwise force on bodies having flat faces of various plan forms; flow normal to flat faces.
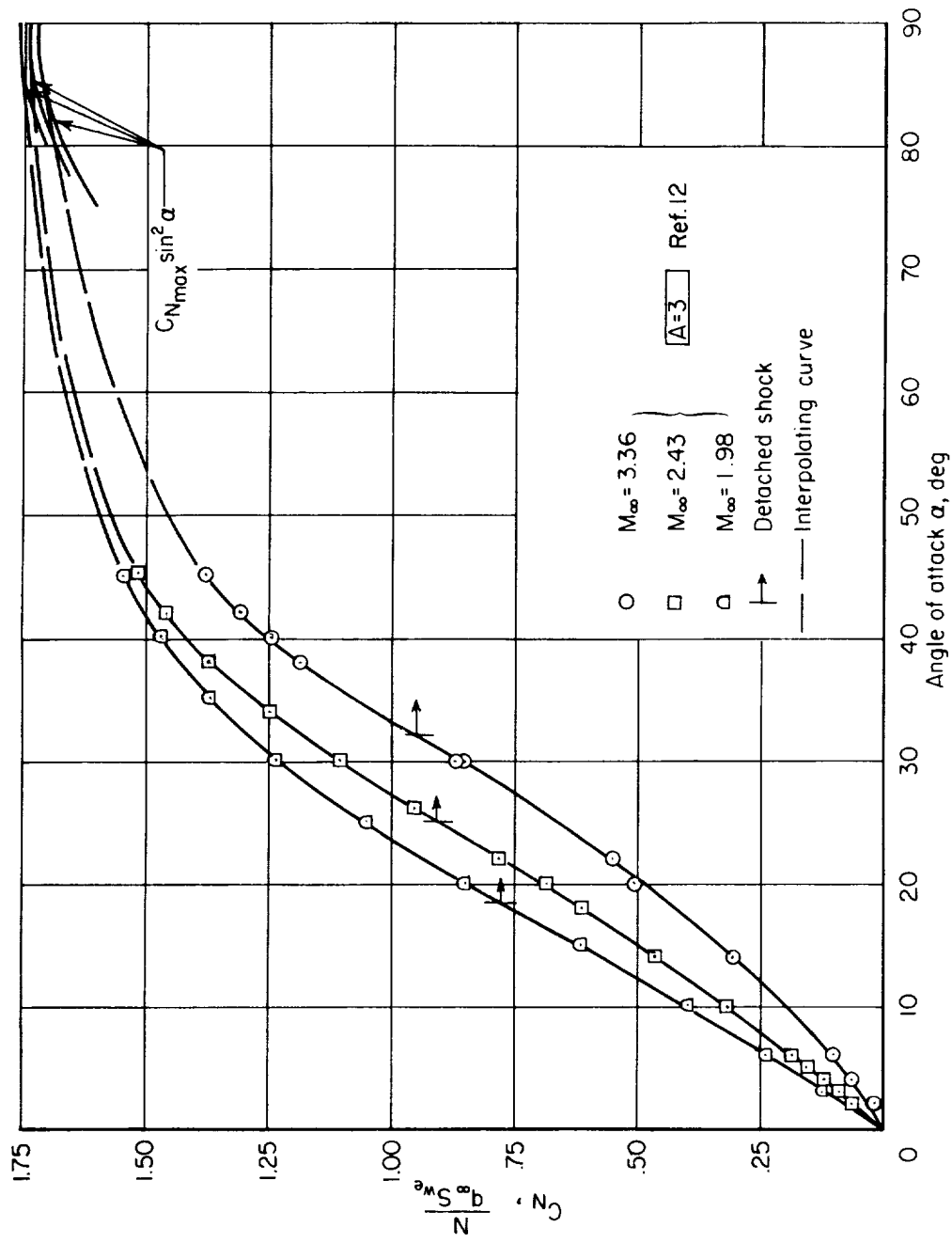
Figure 5.- Normal-force characteristics of a rectangular wing of aspect ratio 3 at angles of attack up to and beyond those for shock detachment for three Mach numbers.
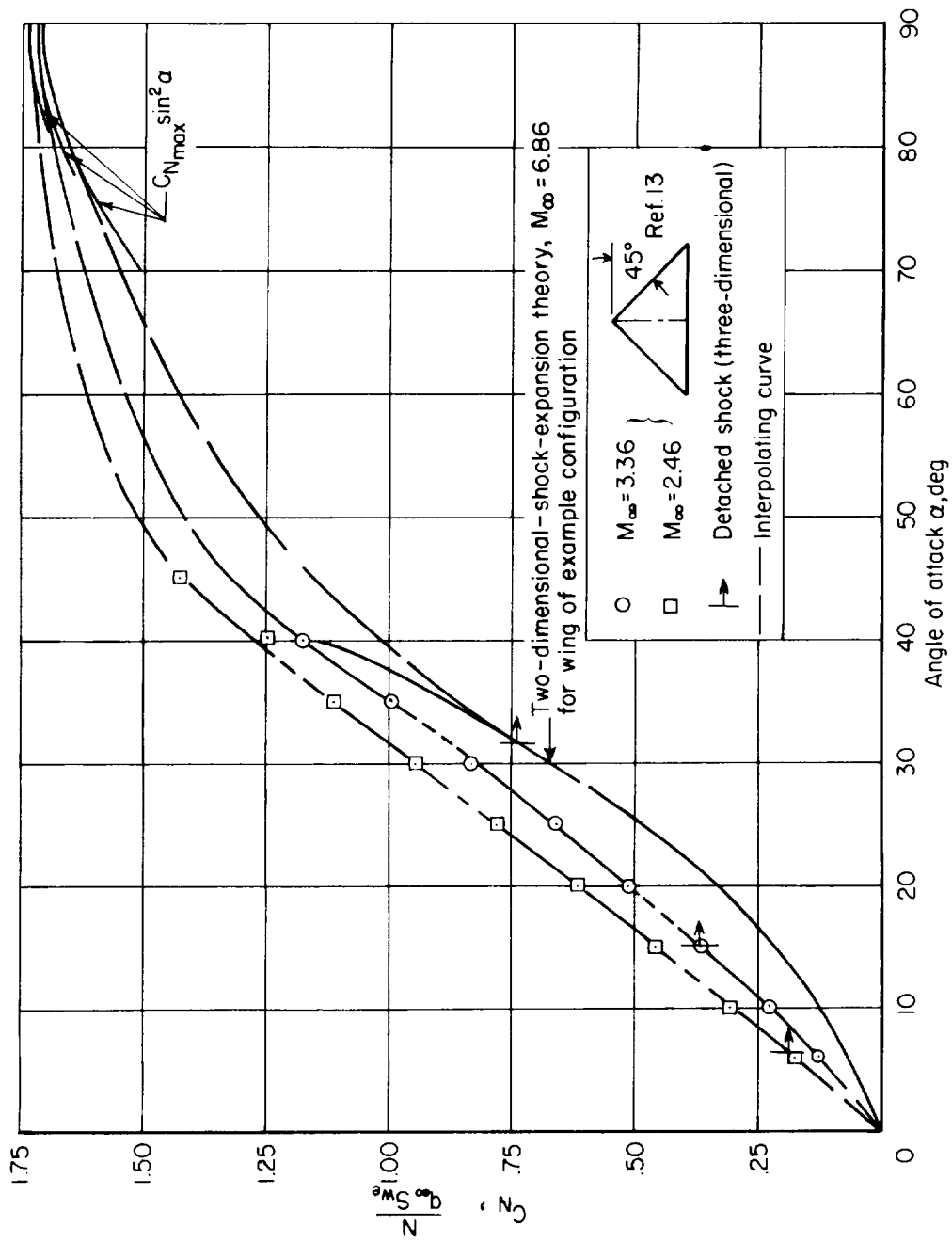
Figure 6.- Estimation of the normal-force characteristics of the isolated wing of the example configuration at $M_{\infty} = 6.86$.
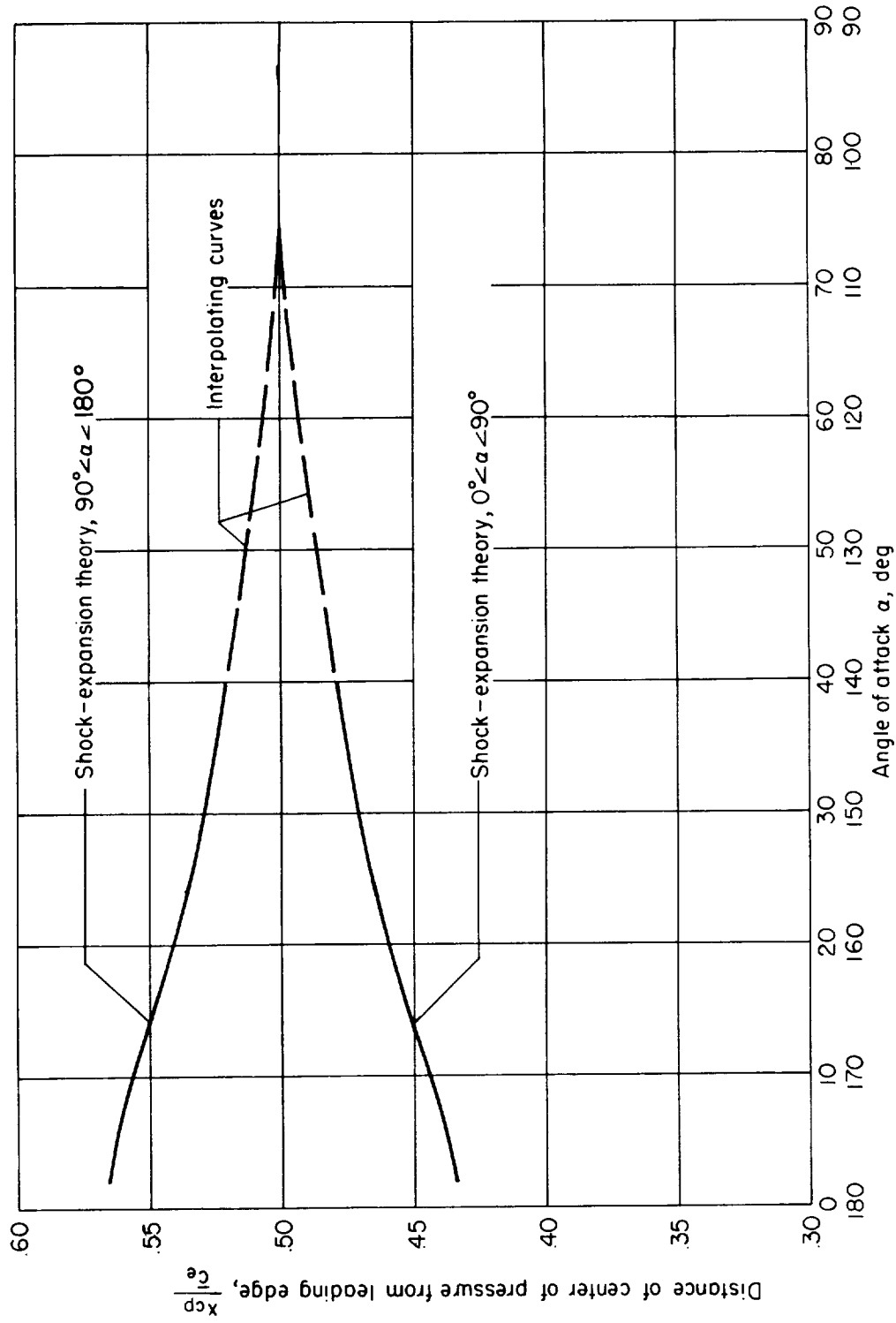
Figure 7.- Estimation of position of the center of pressure for the wing of the example configuration; $M_\infty = 6.86$.
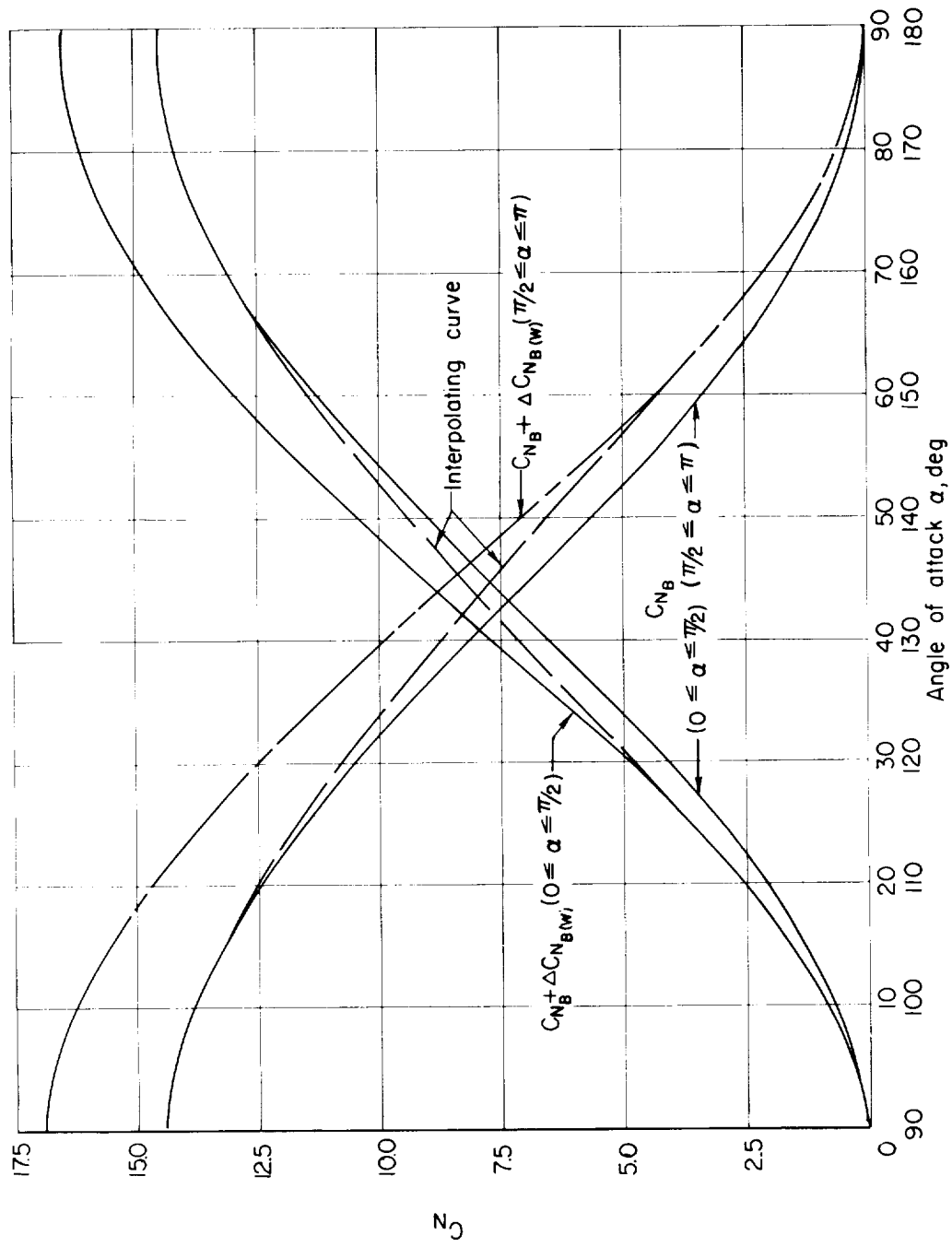
Figure 8.- Estimation of the normal force on the body in the presence of the wing in the case of the example configuration; $M_\infty = 6.86$.
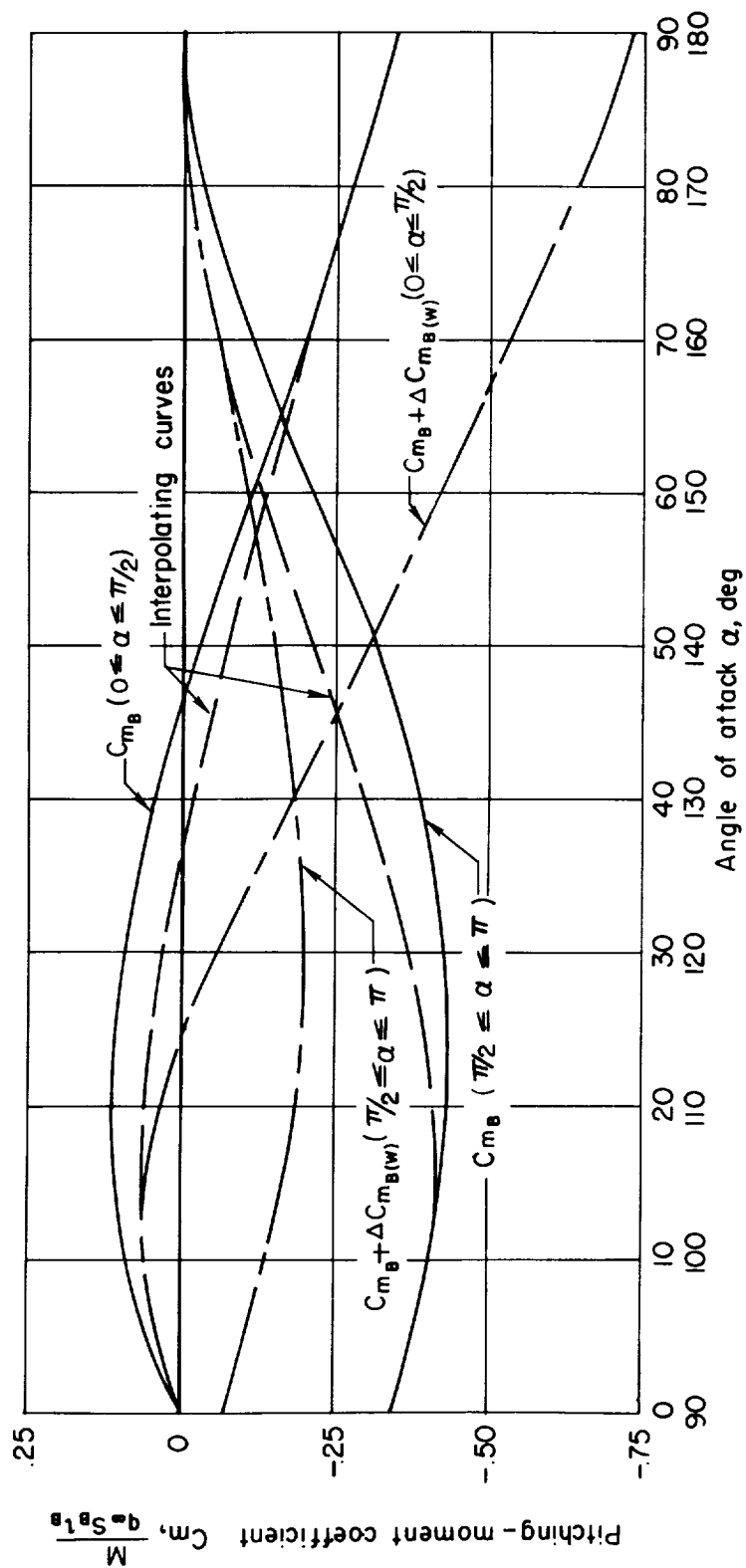
Figure 9.- Estimation of the pitching moment of the body in the presence of the wing in the case of the example configuration; $M_\infty = 6.86$.
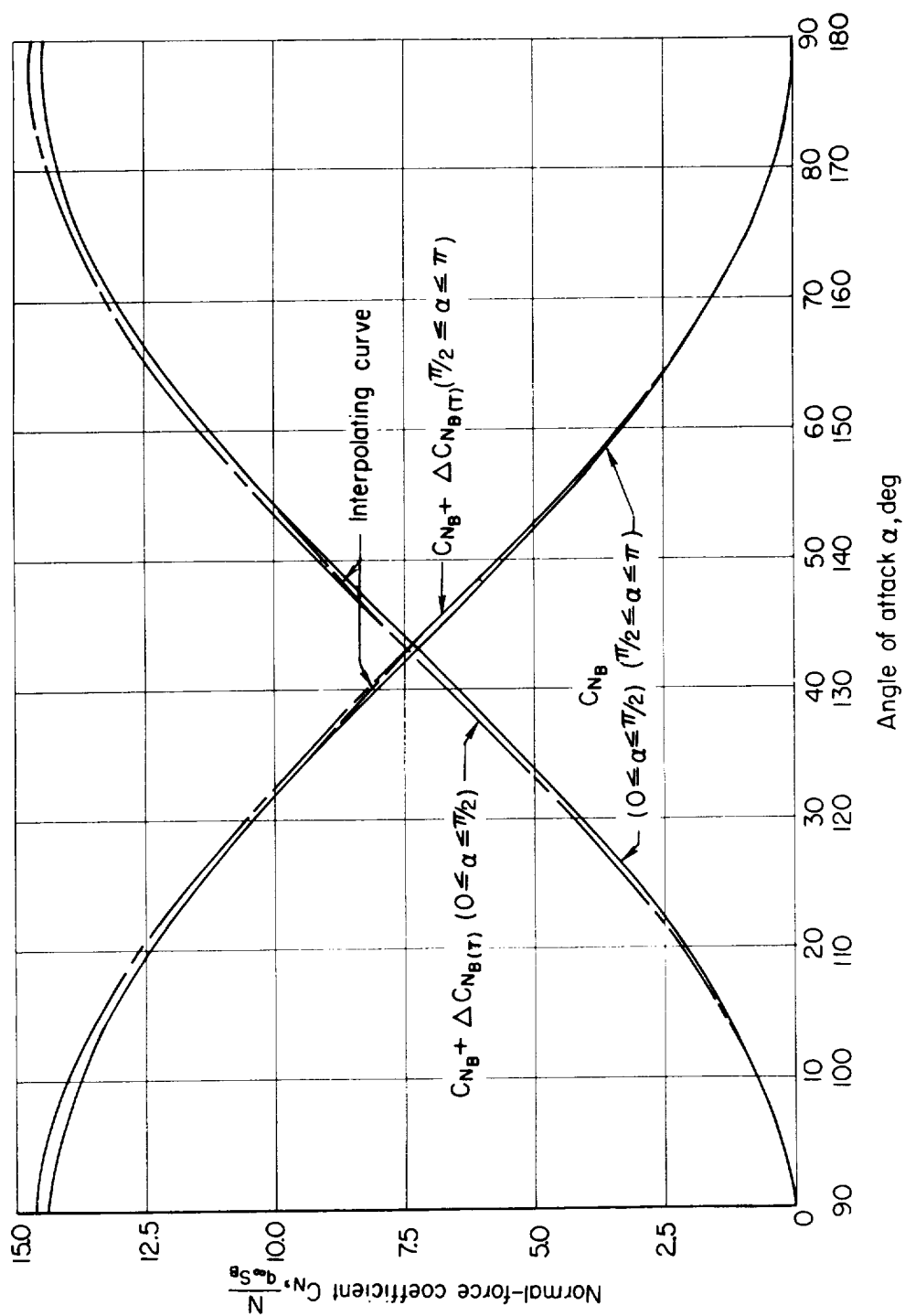
Figure 10.- Estimation of the normal force of the body in the presence of the horizontal tail in the case of the example body-tail configuration; $M_\infty = 6.86$.
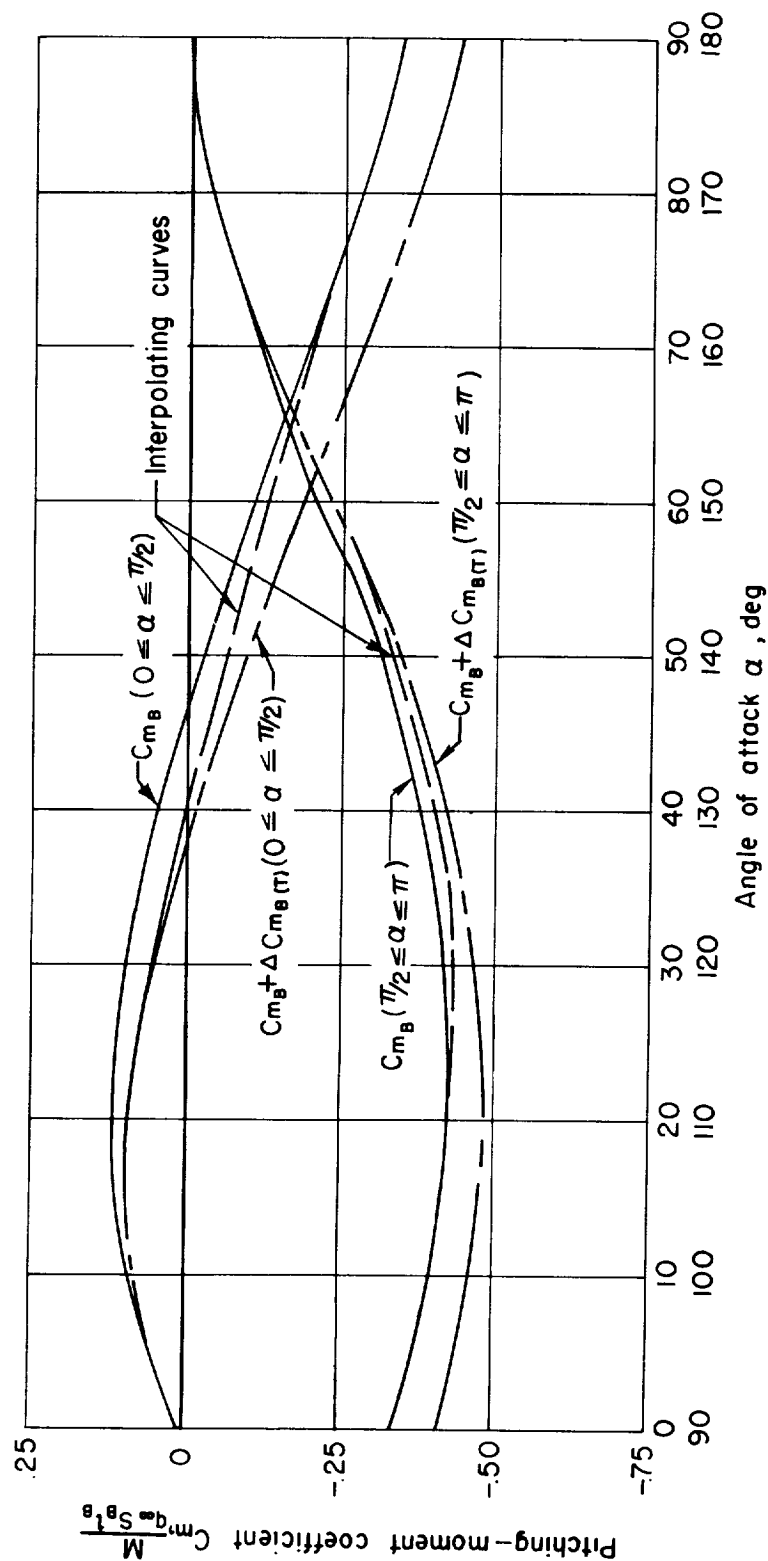
Figure 11.- Estimation of the pitching moment of the body in the presence of the horizontal tail in the case of the example body-tail configuration; $M_\infty = 6.86$.
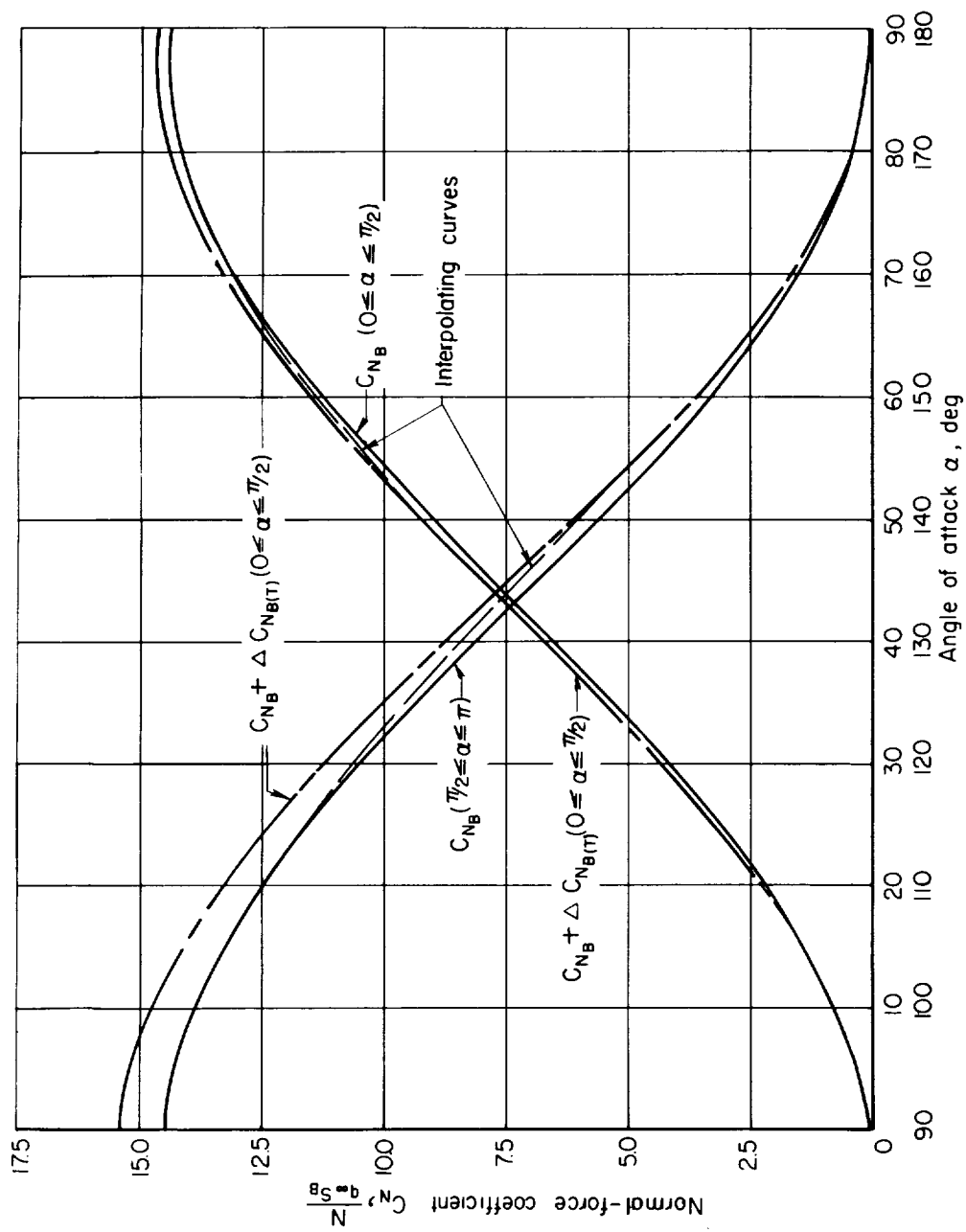
Figure 12.- Estimation of the normal force of the body in the presence of the horizontal tail in the case of the example body-wing-tail configuration; $M_\infty = 6.86$.
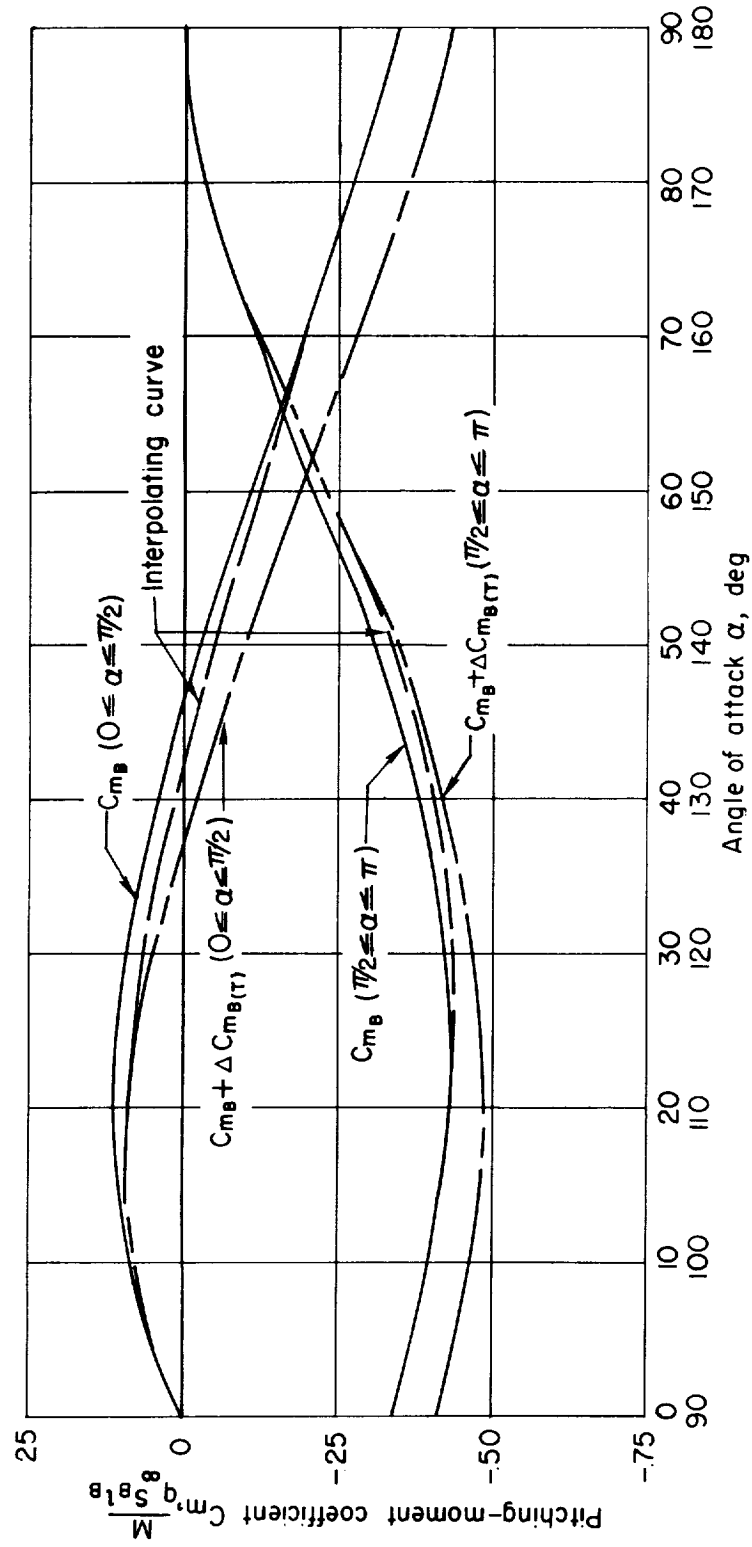
Figure 13.- Estimation of the pitching moment of the body in the presence of the horizontal tail in the case of the example body-wing-tail configuration; $M_\infty = 6.86$.
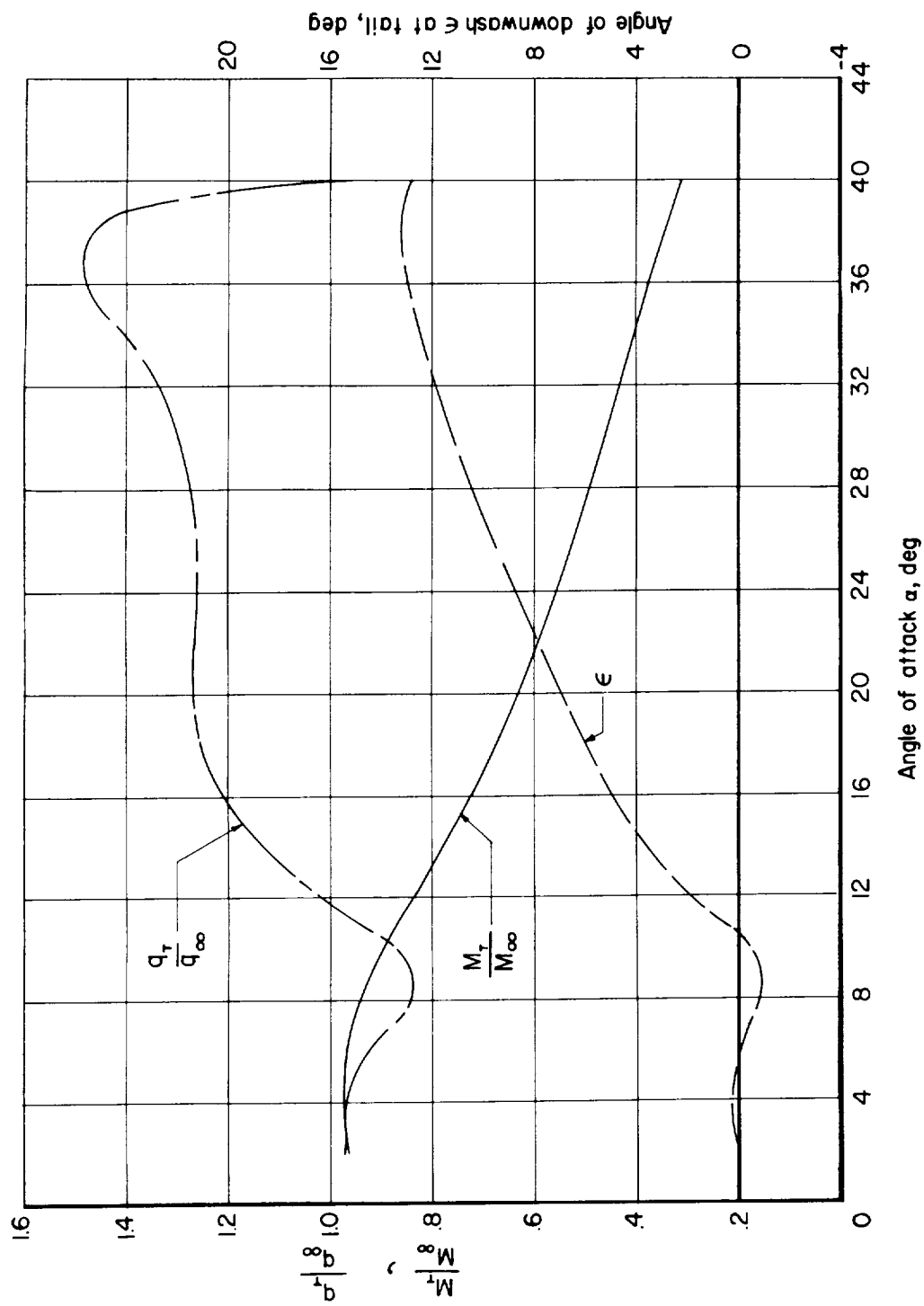
Figure 14.- Flow characteristics in region of tail in the wake of the wing of the example configuration; $M_\infty = 6.86$.
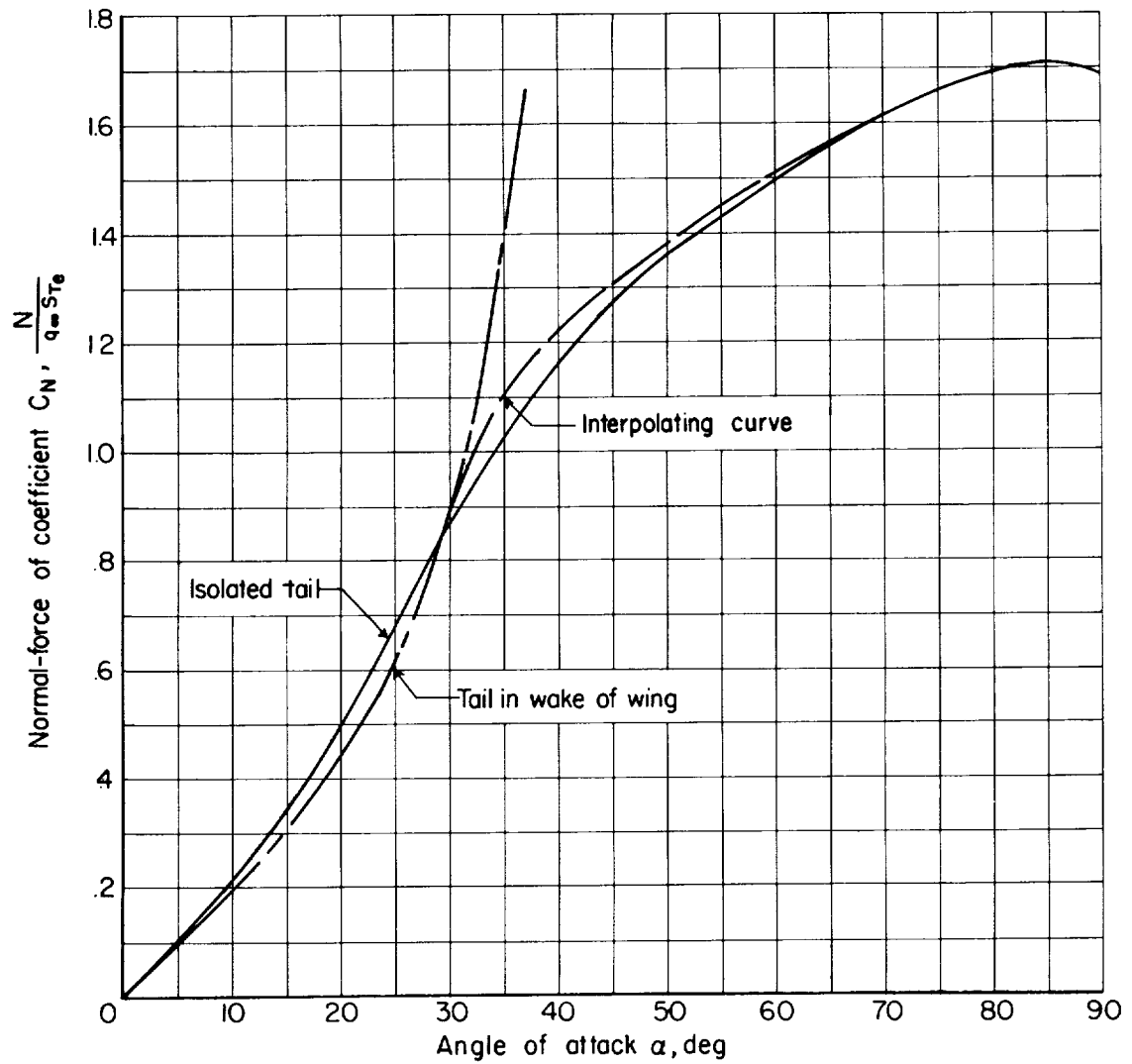
Figure 15.- Estimation of the normal force of the tail in the wake of the wing in the case of the example configuration; $M_\infty = 6.86$.
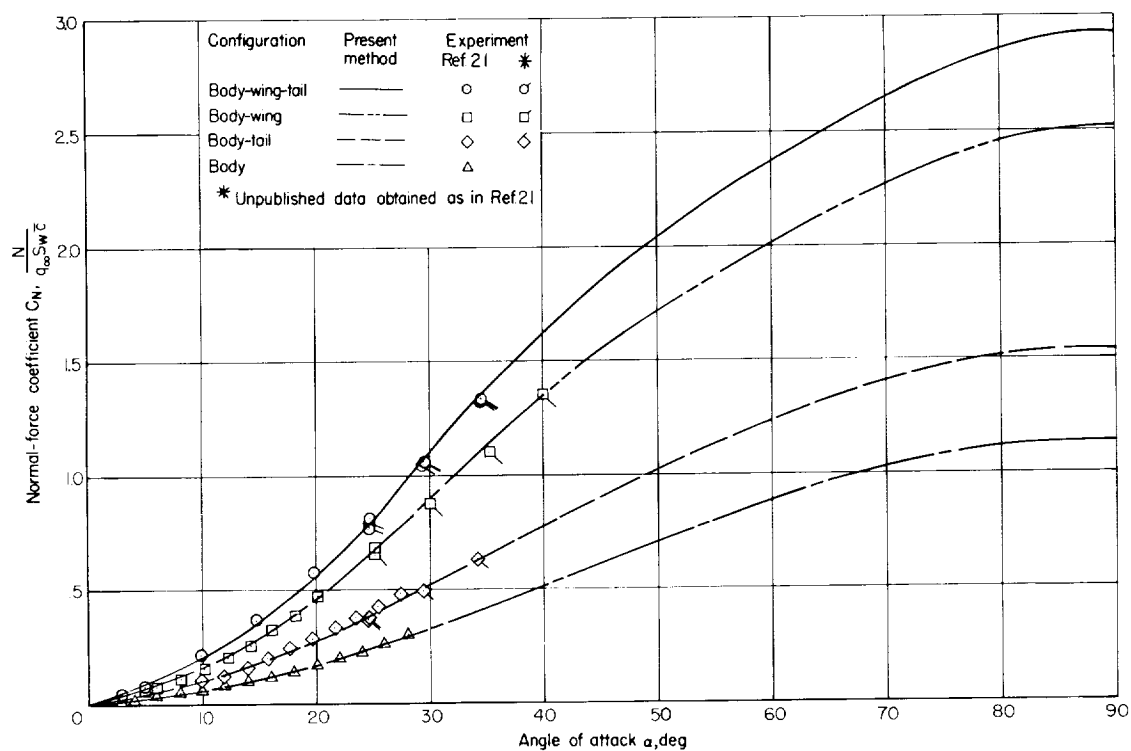
Figure 16.- Variation of normal-force coefficient with angle of attack for the example airplane configuration and its components; $M_\infty = 6.86$.
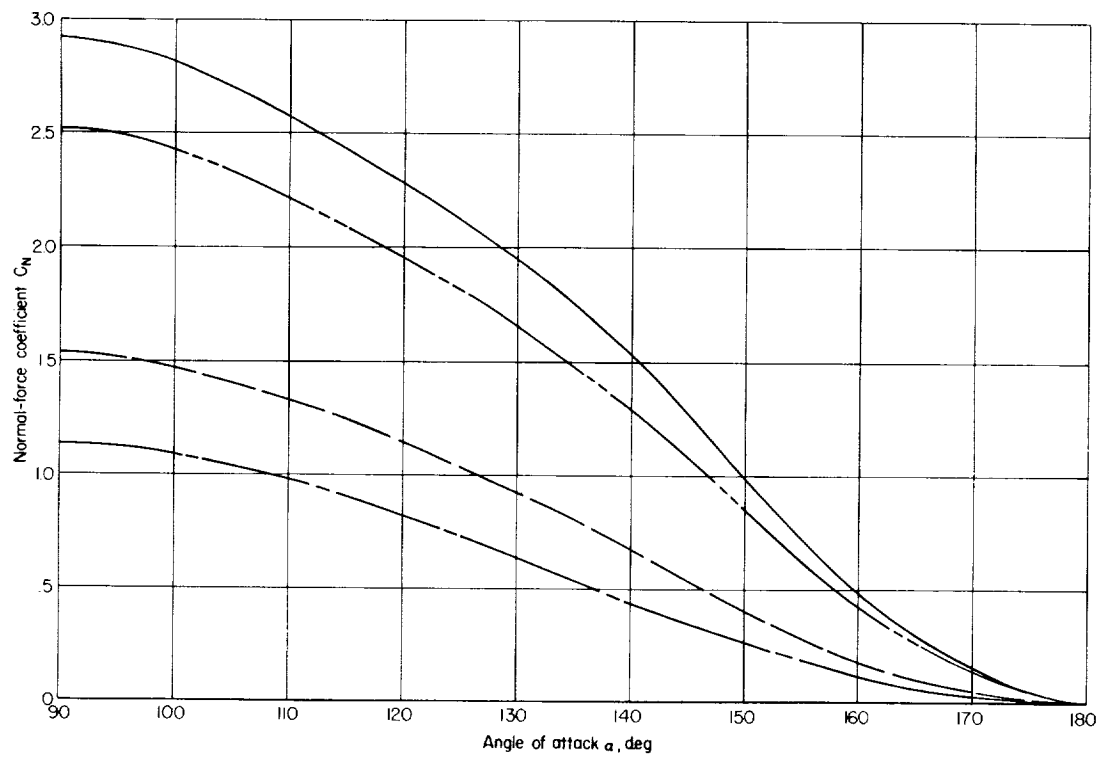
Figure 16.- Concluded.
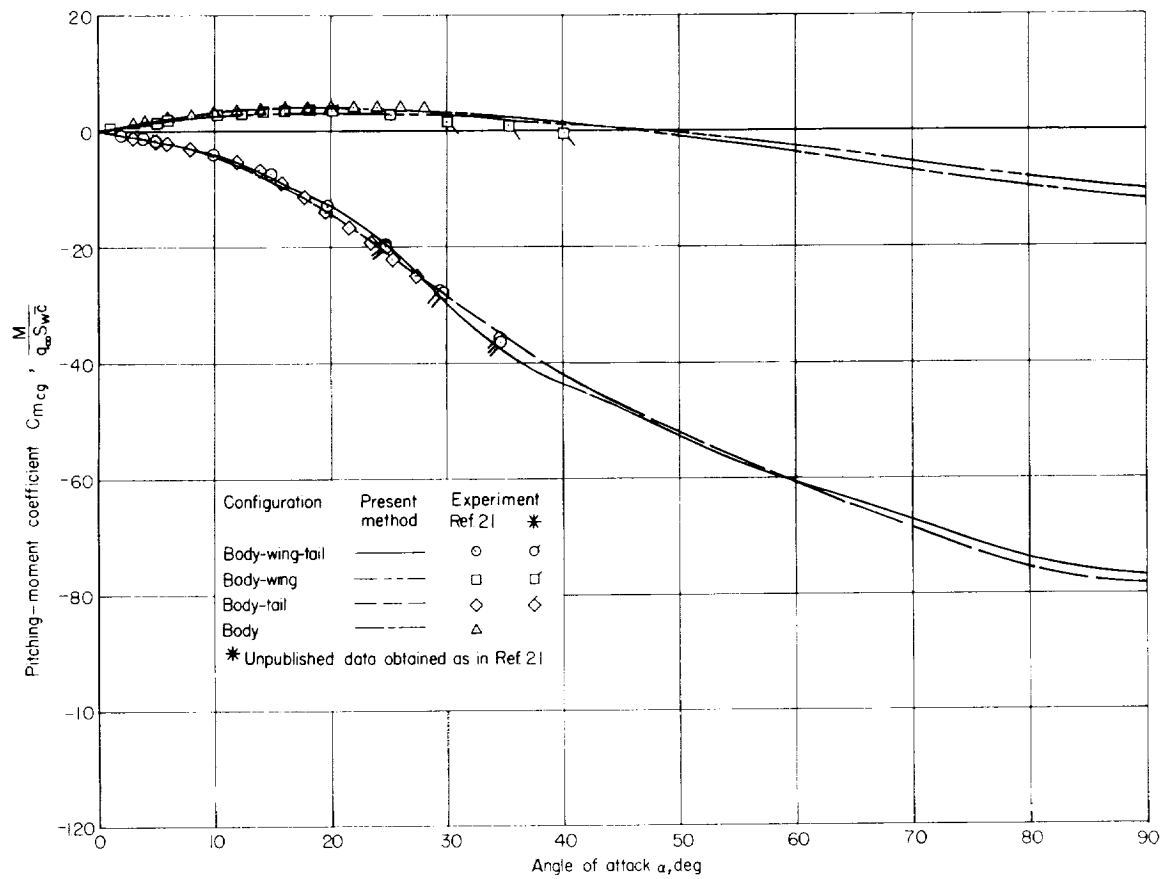
Figure 17.- Variation of pitching-moment coefficient with angle of attack for the example airplane configuration and its components; $M_\infty = 6.86$.
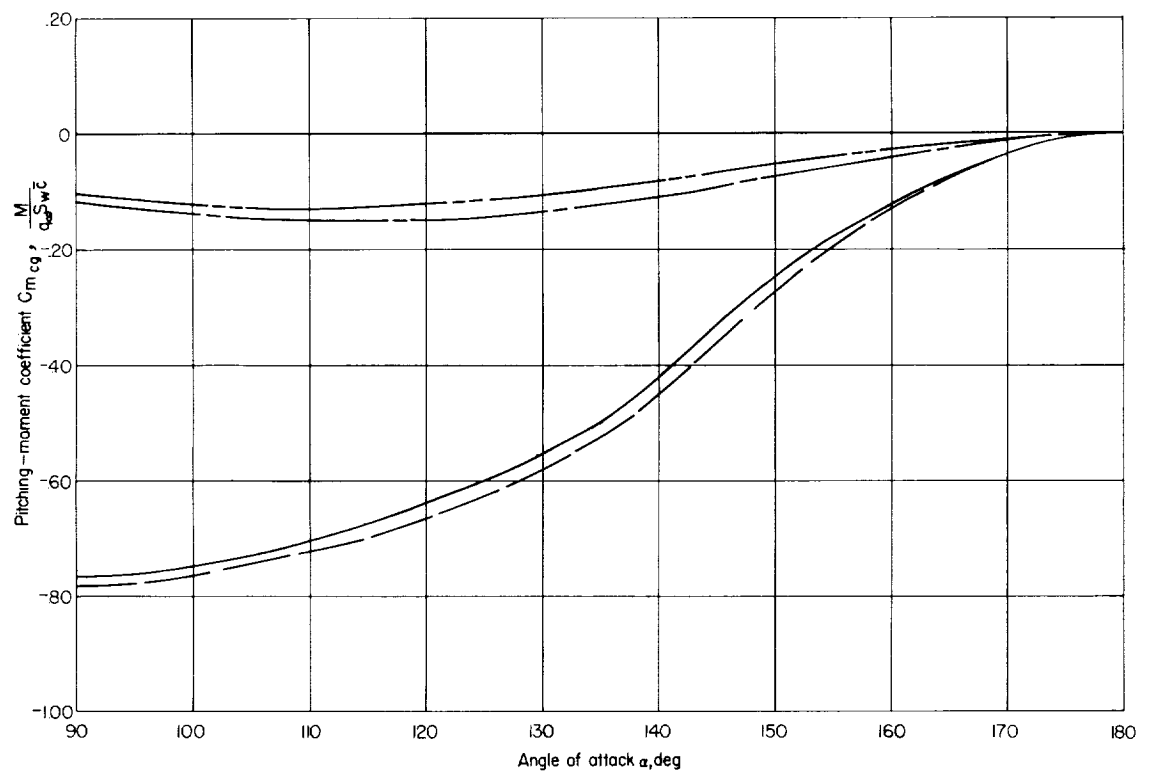
Figure 17.- Concluded.
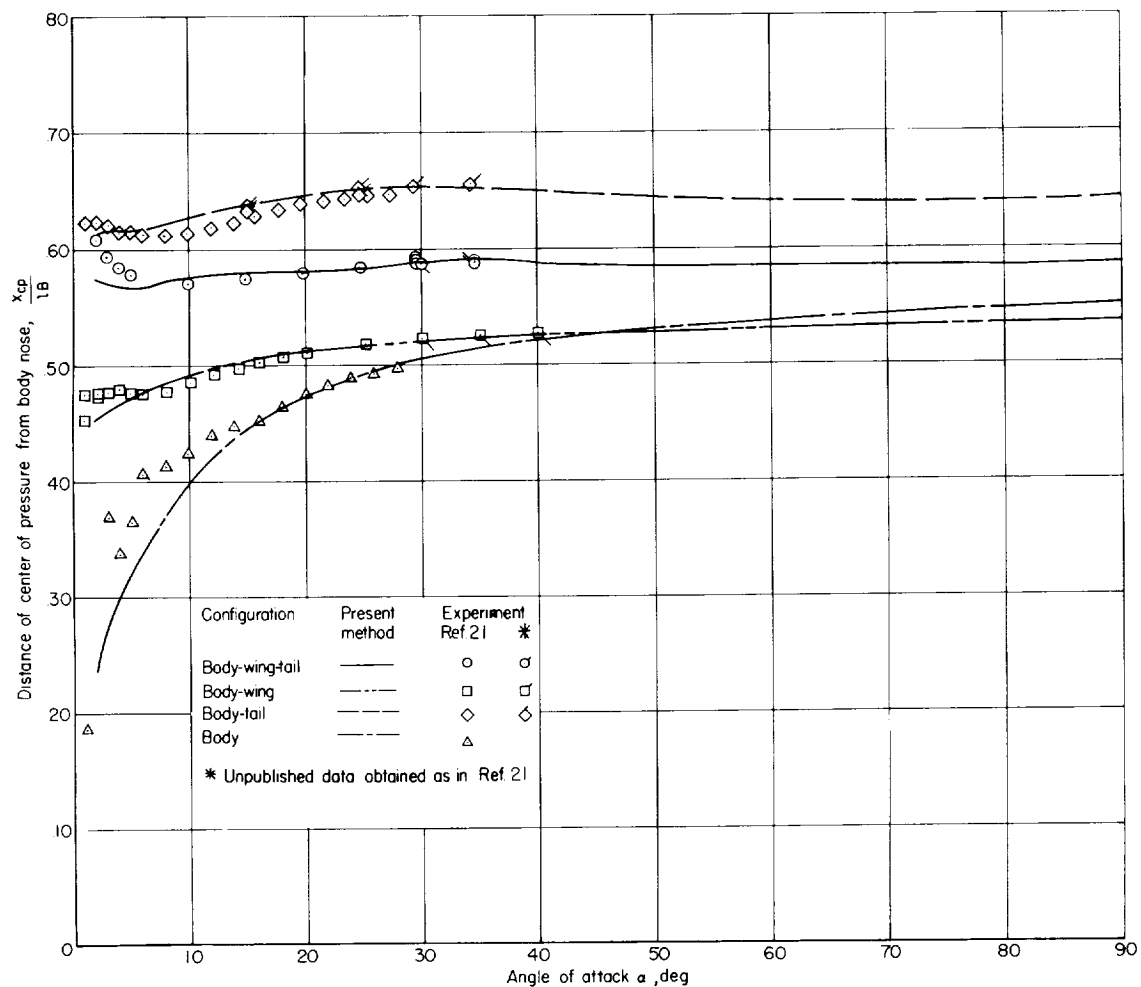
Figure 18.- Variation of location of center of pressure with angle of attack for example airplane configuration and its components; $M_\infty = 6.86$.
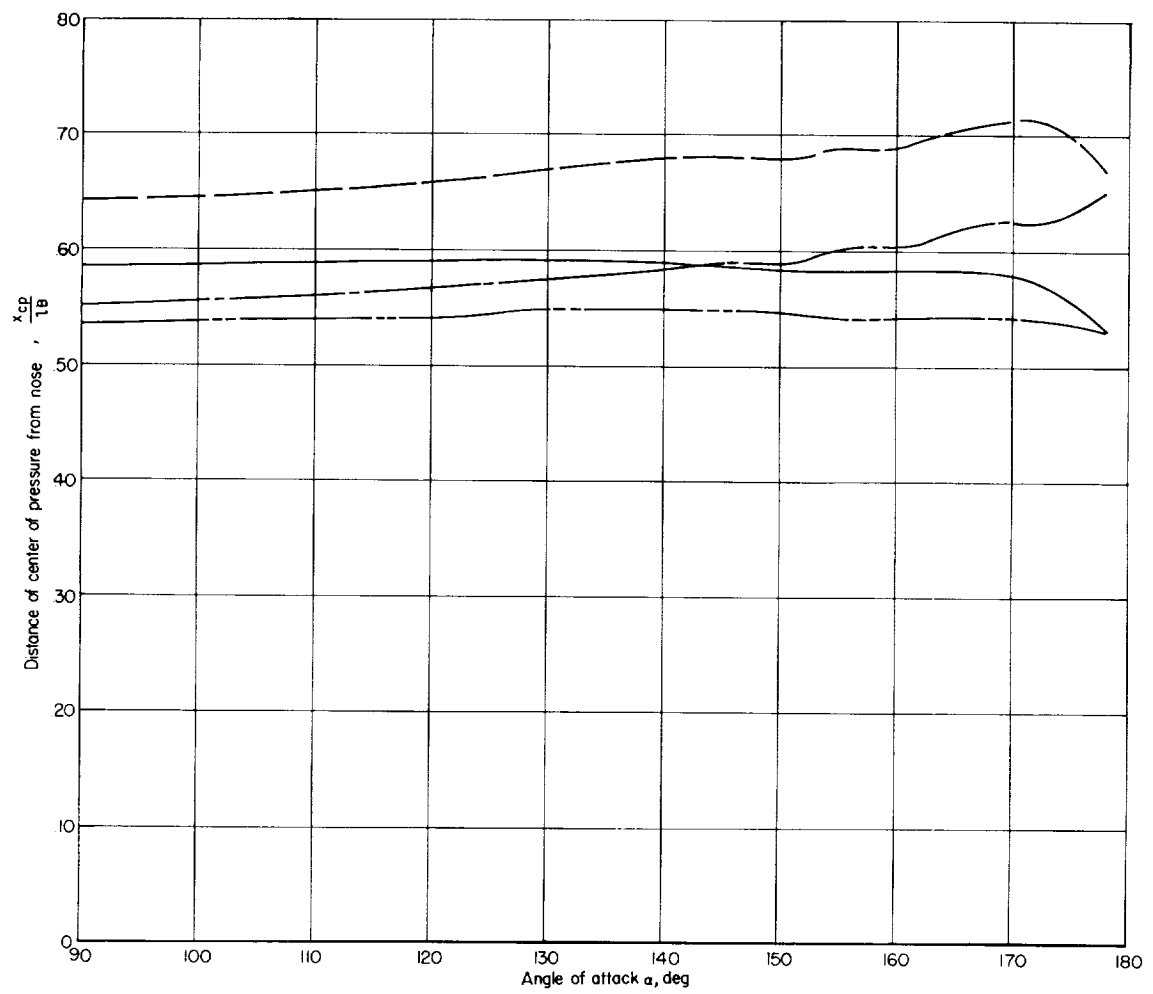
Figure 18.- Concluded.
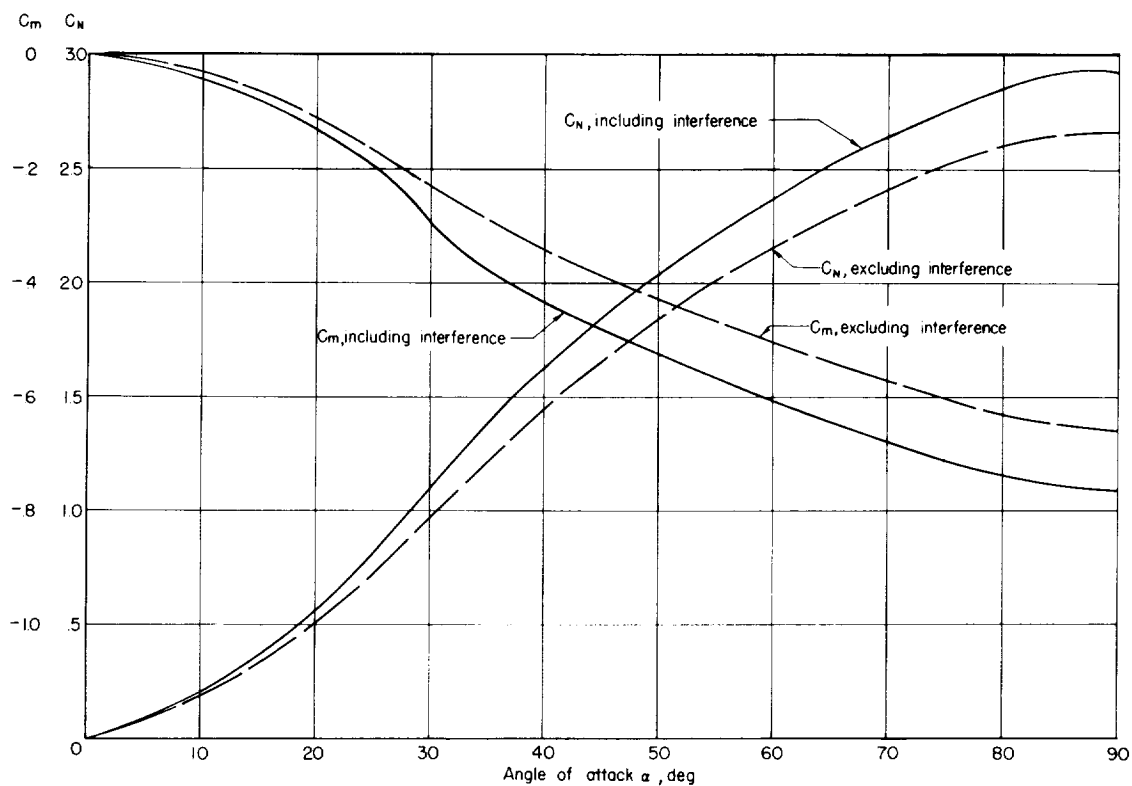
Figure 19.- Comparison between results obtained by including and neglecting interference effects in estimating normal force and pitching moment for example airplane configuration; M_∞ = 6.86.
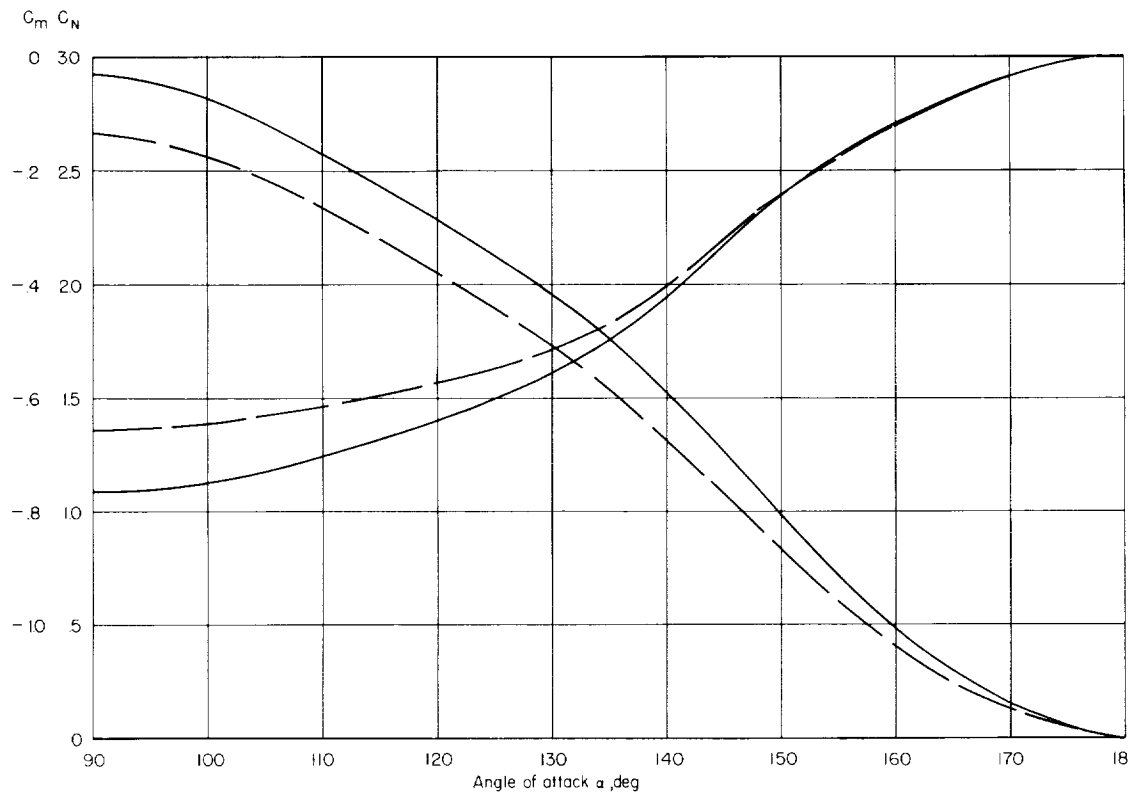
Figure 19.- Concluded.
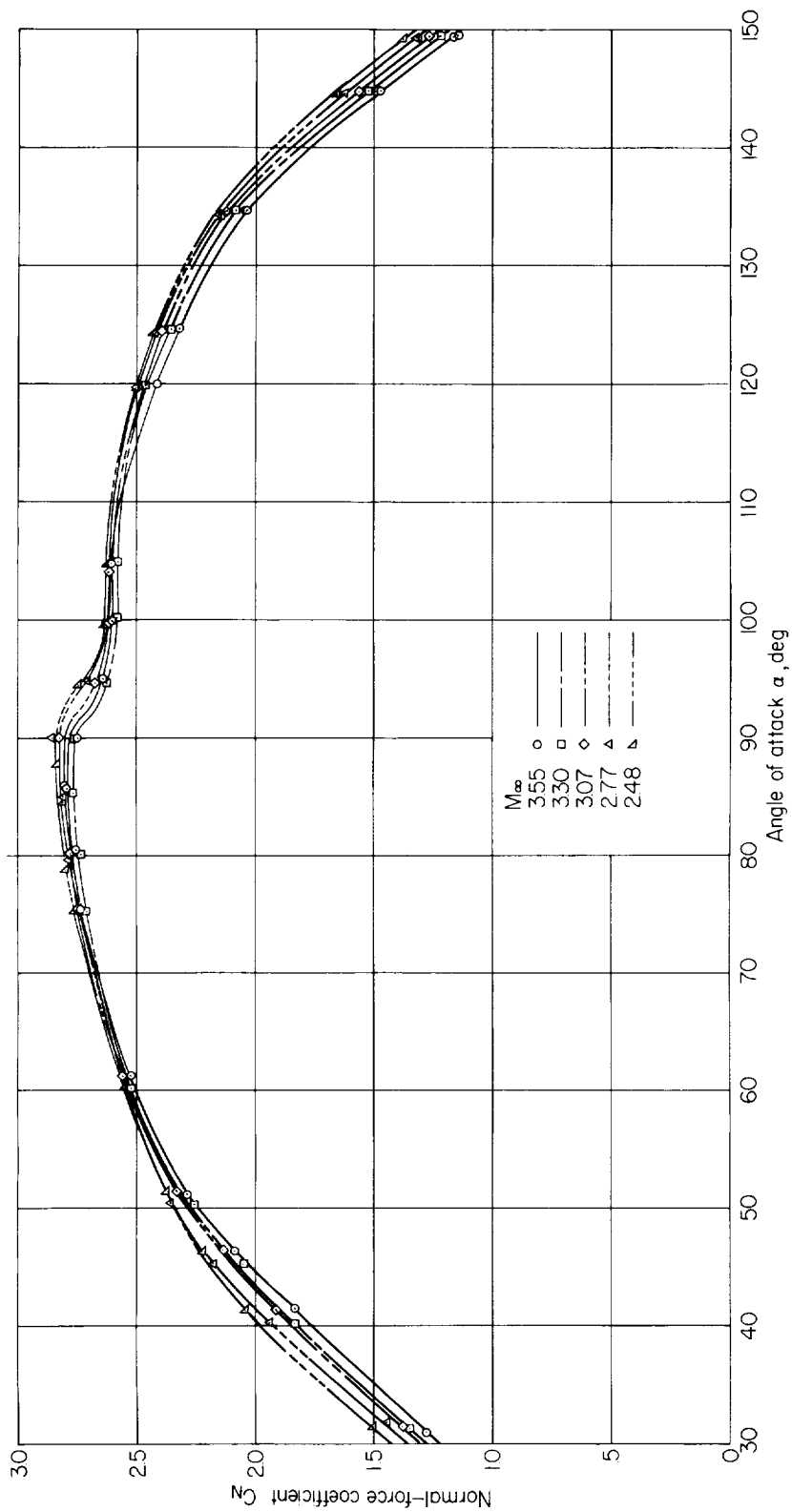
Figure 20.- Experimental variation of normal-force coefficient with angle of attack for example airplane configuration at five supersonic Mach numbers.
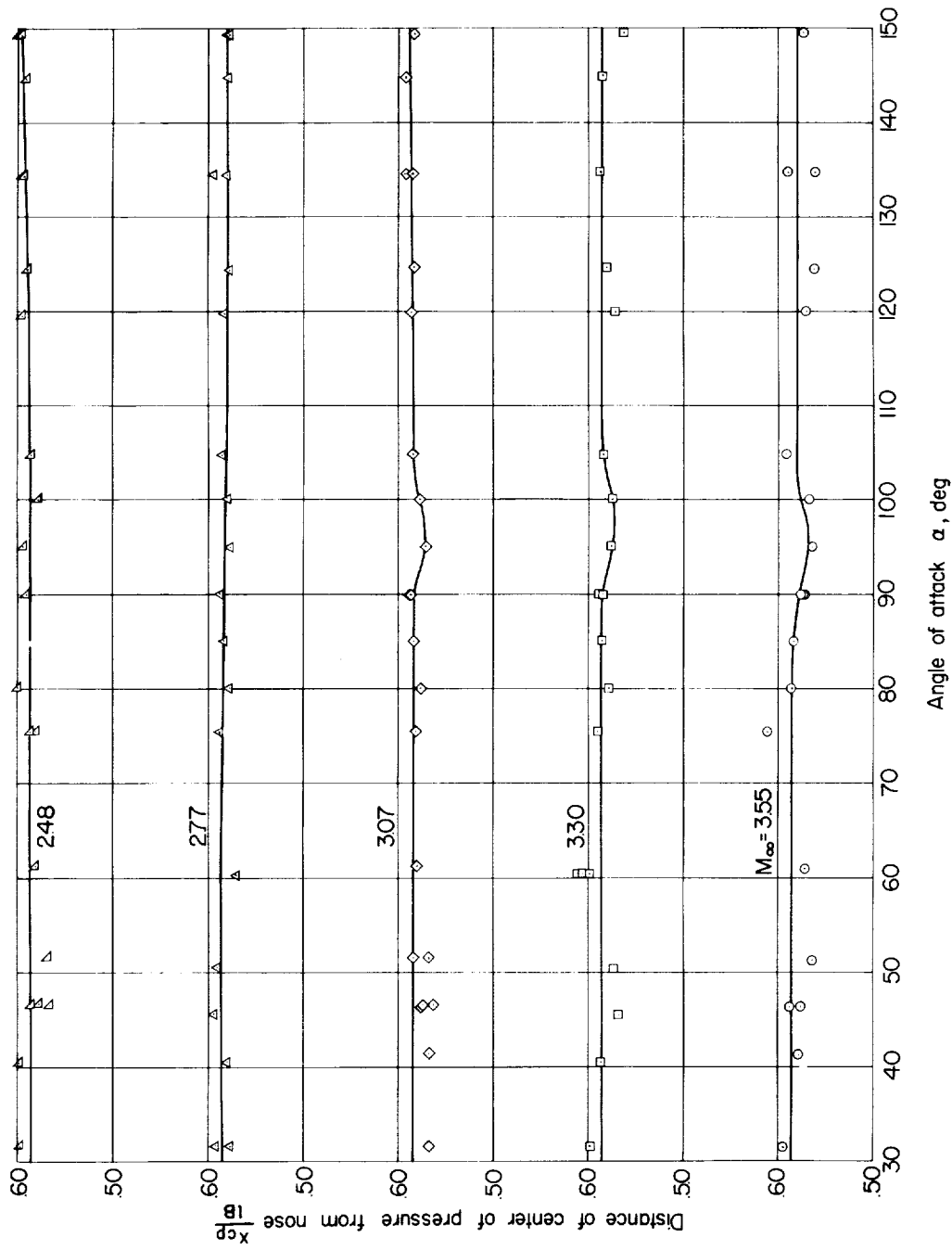
Figure 21.- Experimental variation of center-of-pressure location with angle of attack for example airplane configuration at five supersonic Mach numbers.
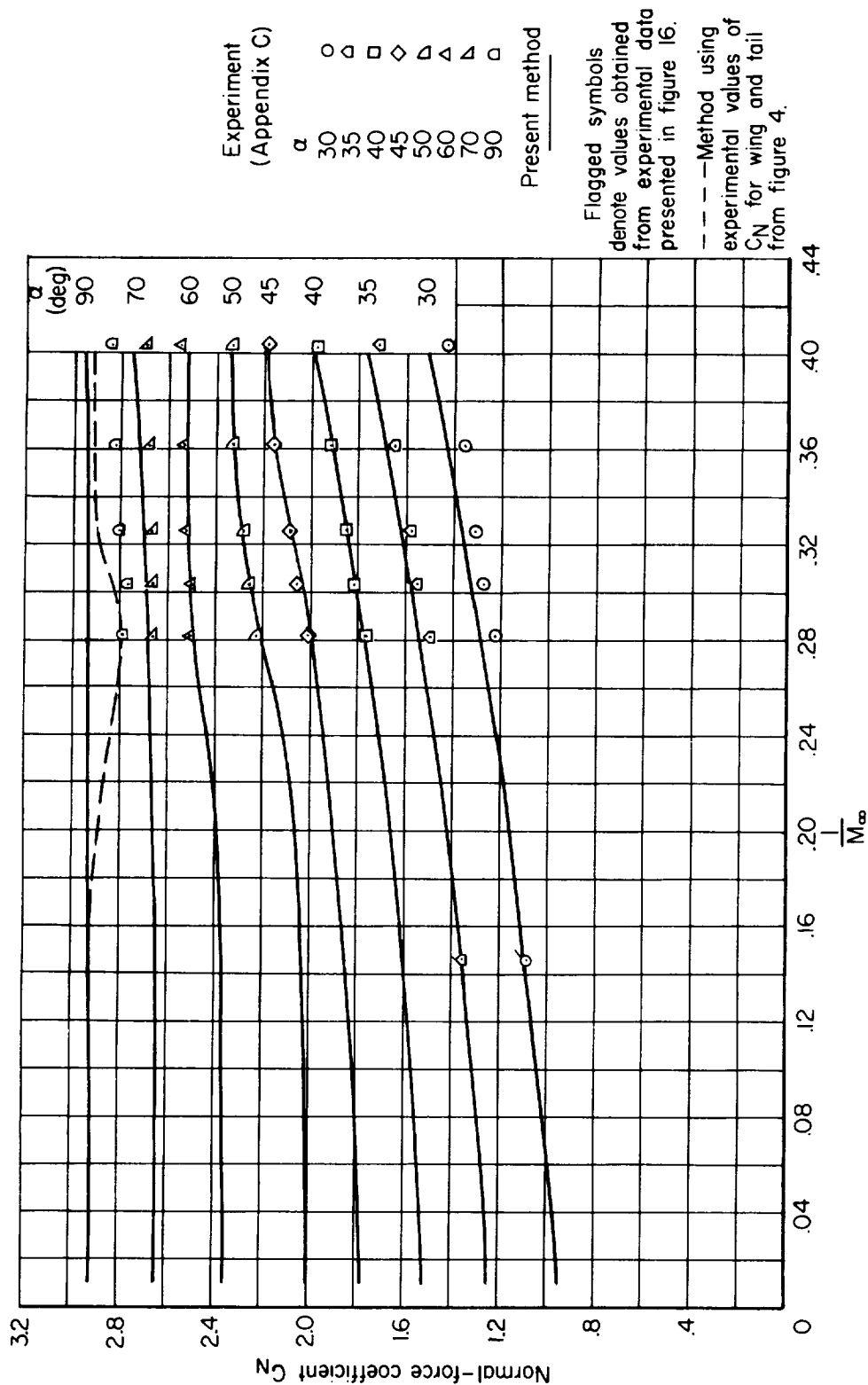
Figure 22.- Estimated and experimental variation of normal-force coefficient of example airplane configuration with Mach number at a number of angles of attack.
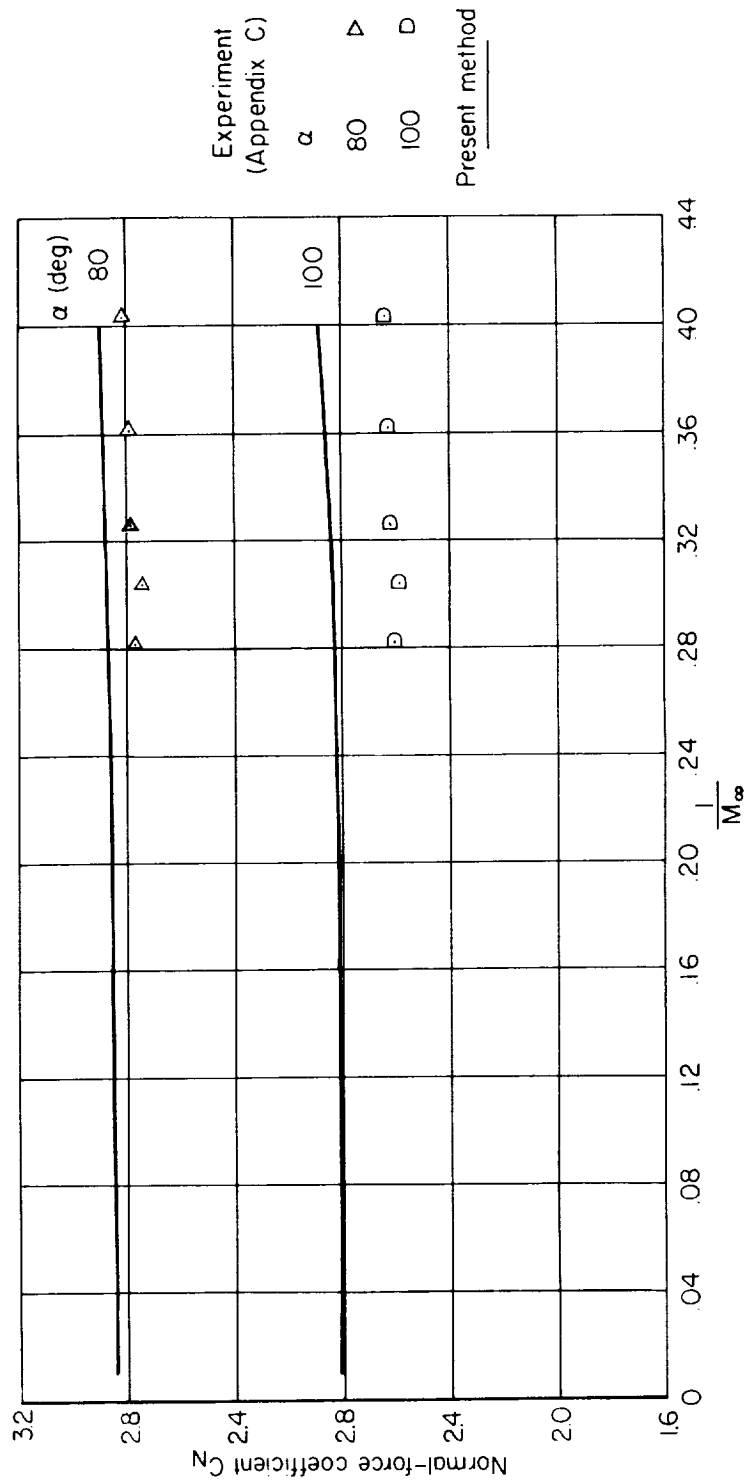
Figure 22. - Continued.
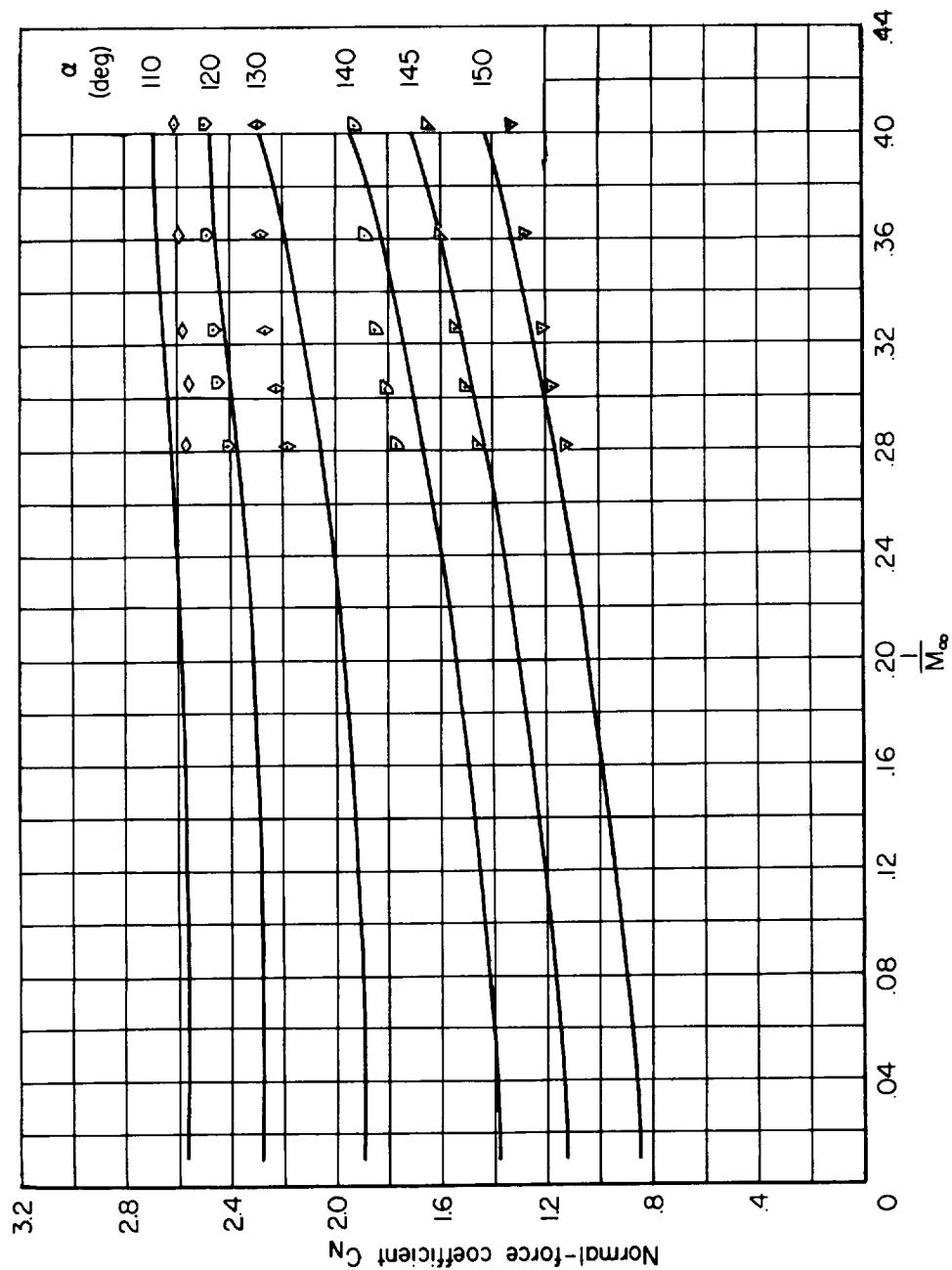
Figure 22.- Concluded.
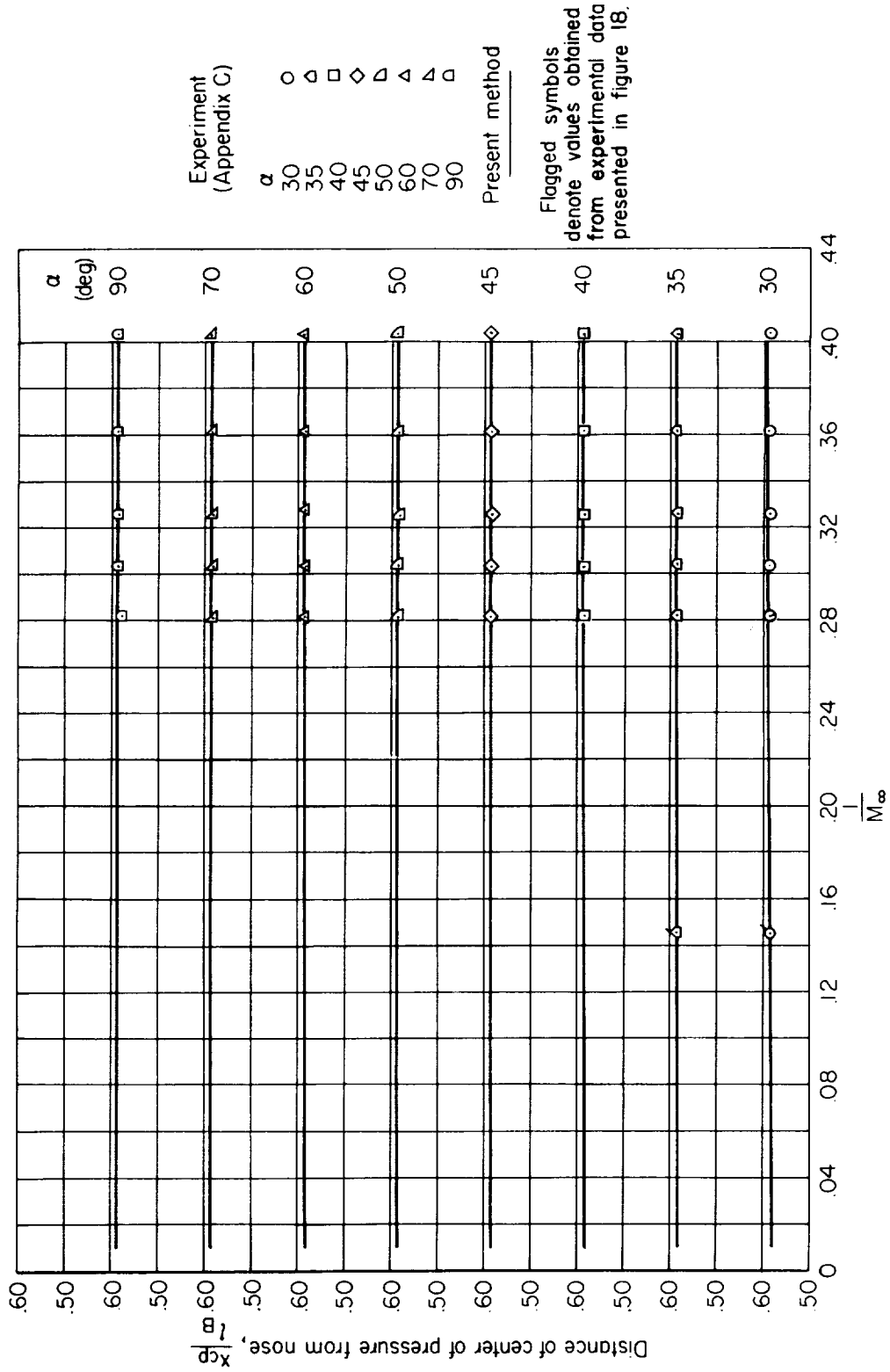
Figure 23.- Estimated and experimental variation of center-of-pressure location with Mach number for example airplane configuration at a number of angles of attack.
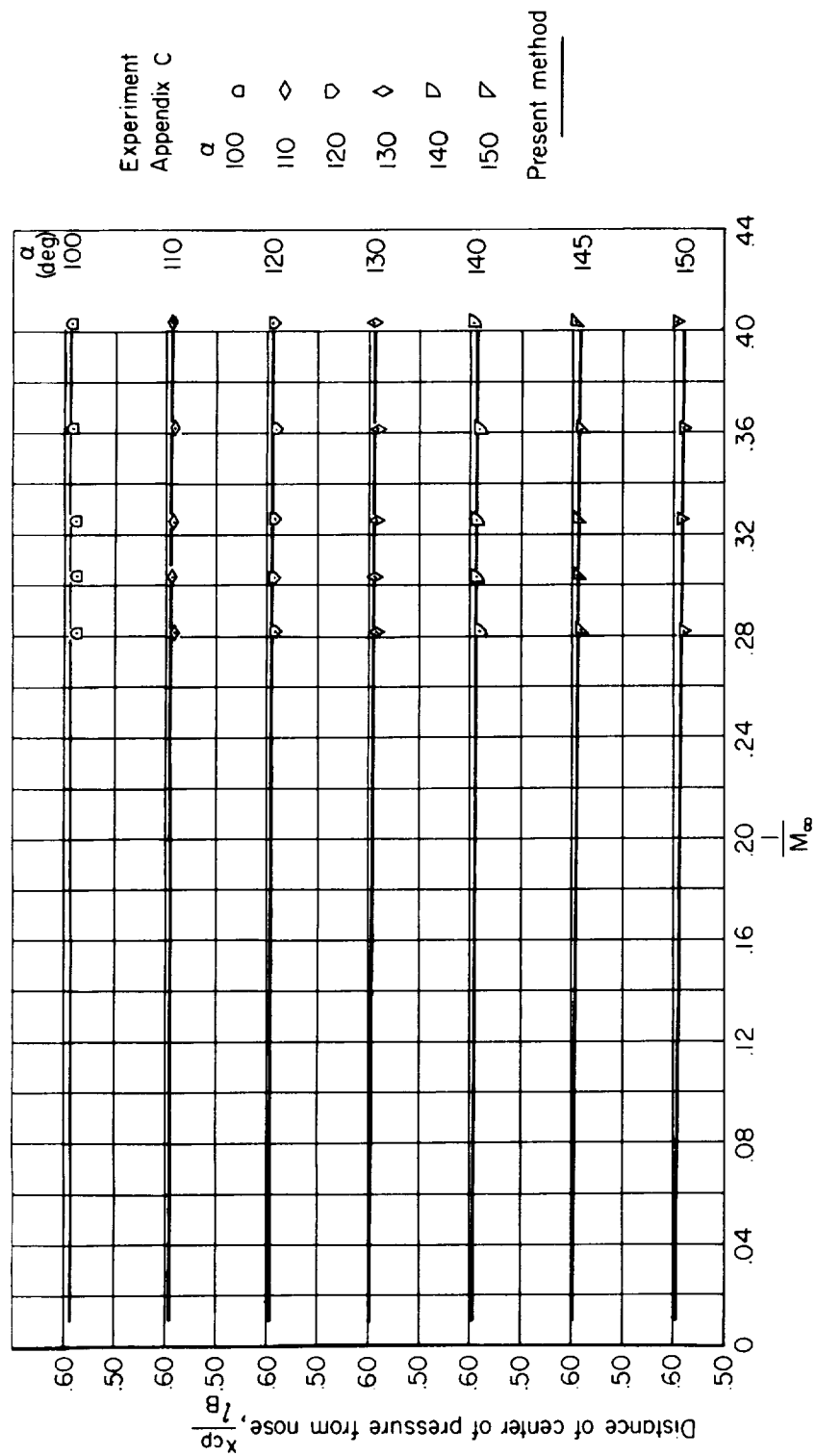
Figure 23.- Concluded.
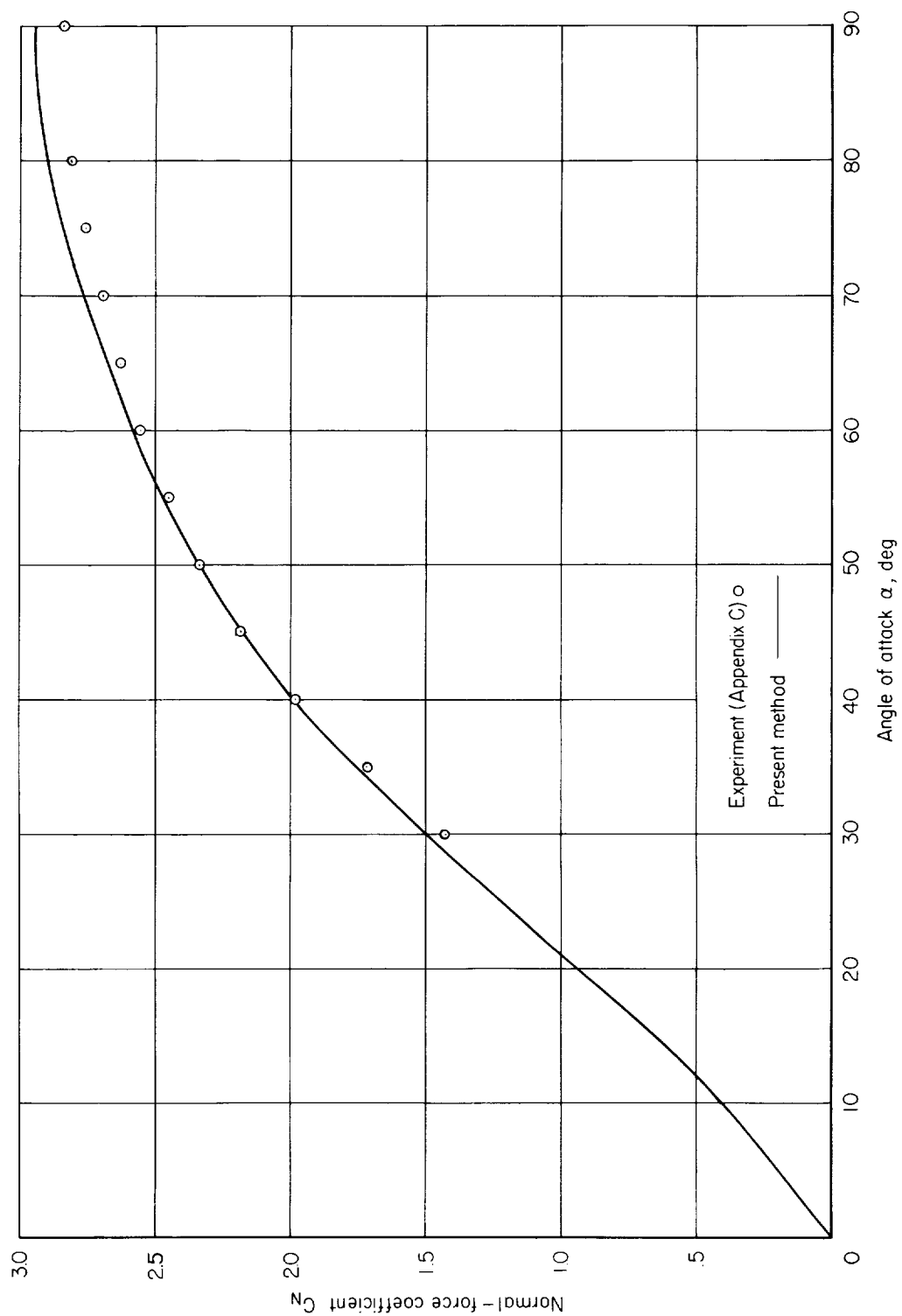
Figure 24.- Variation of normal-force coefficient of example airplane configuration with angle of attack; $M_\infty = 2.5$.
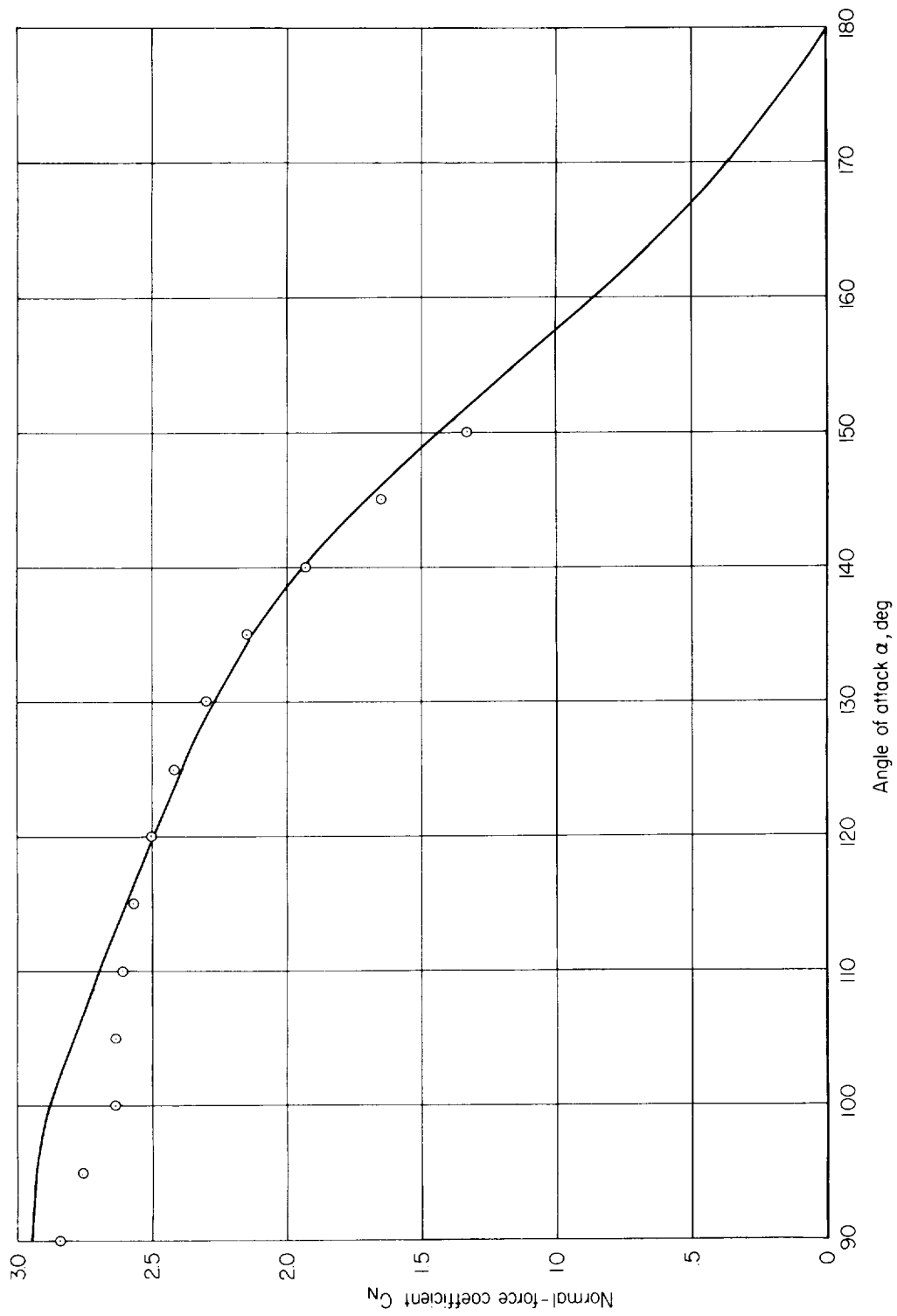
Figure 24.- Concluded.
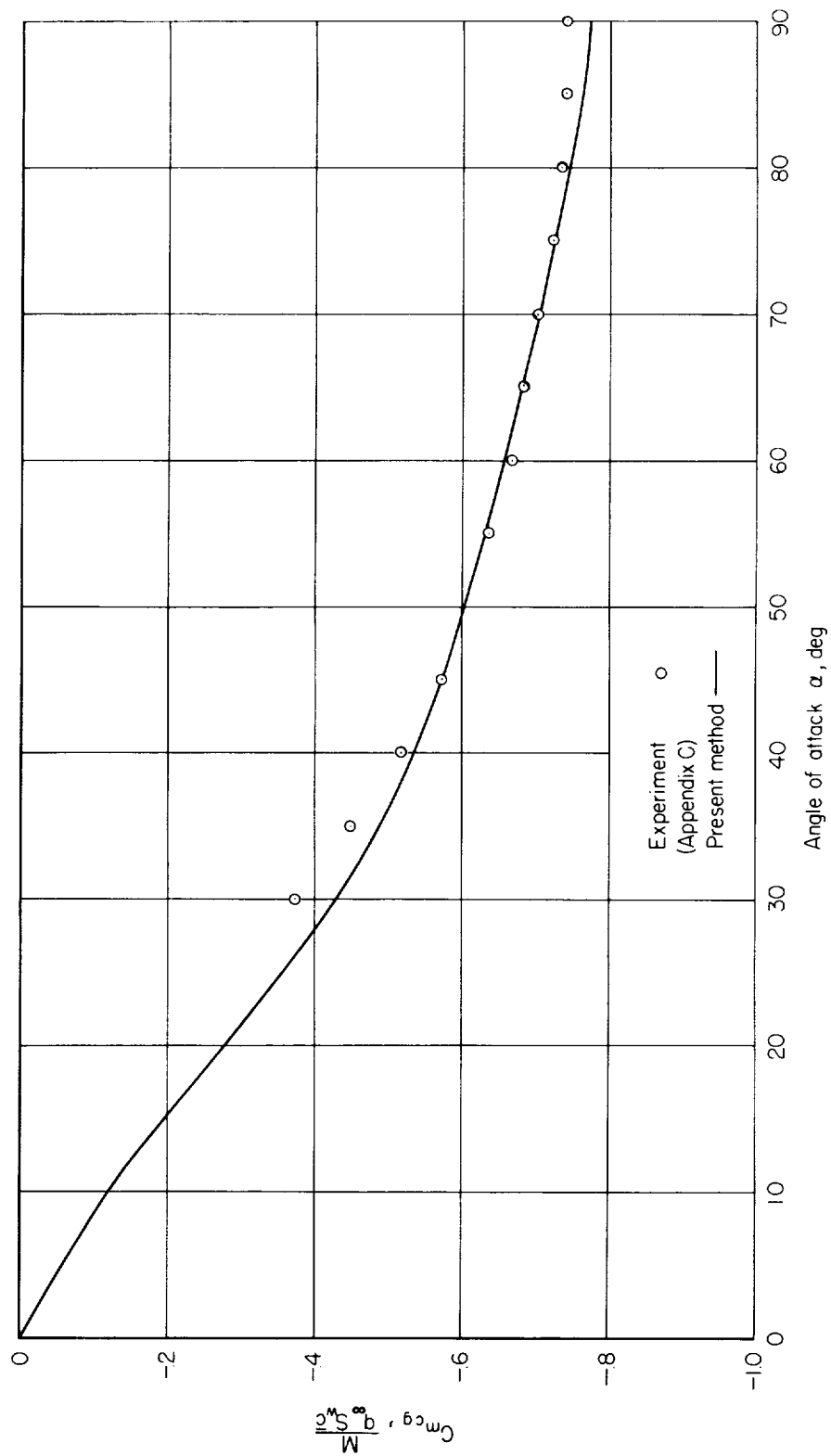
Figure 25.- Variation of pitching-moment coefficient of example airplane configuration with angle of attack; $M_\infty = 2.5$.
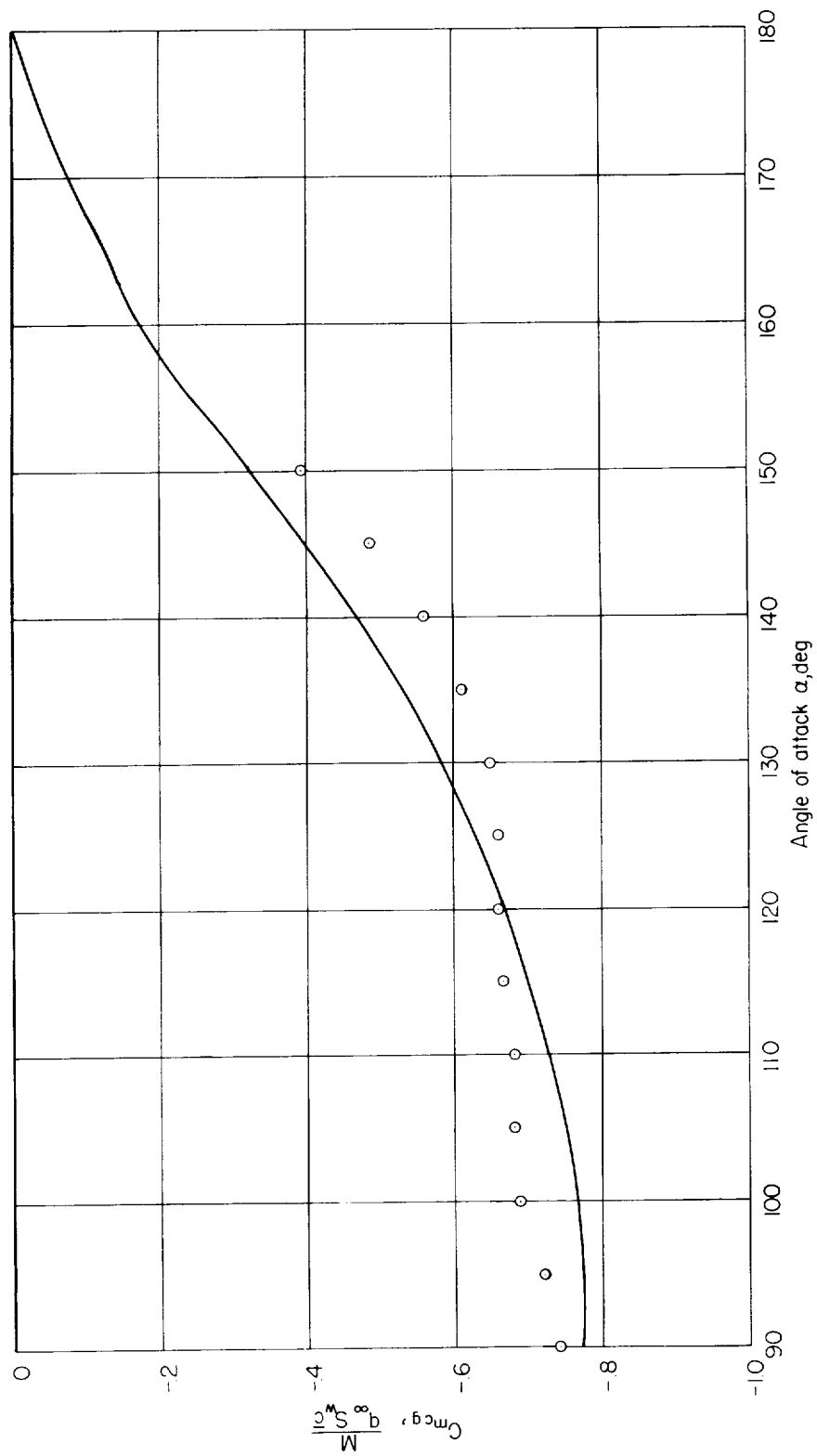
Figure 25.- Concluded.

71
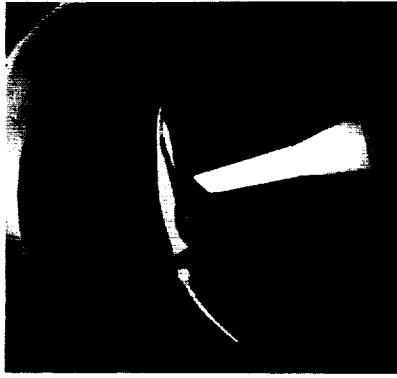
$\alpha = 75^\circ$
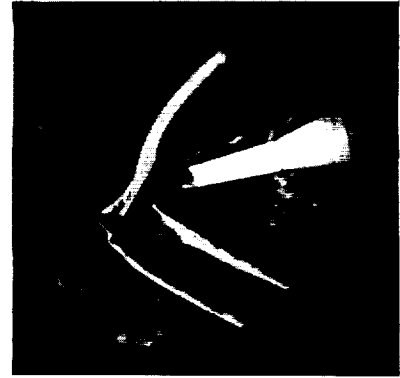
$\alpha = 120^\circ$
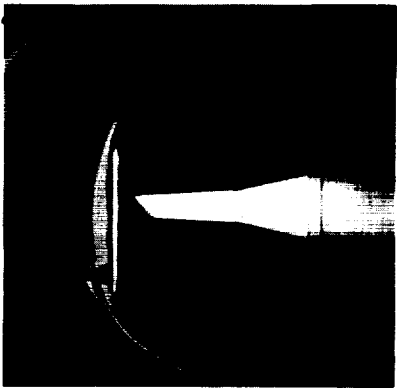
$\alpha = 90^\circ$
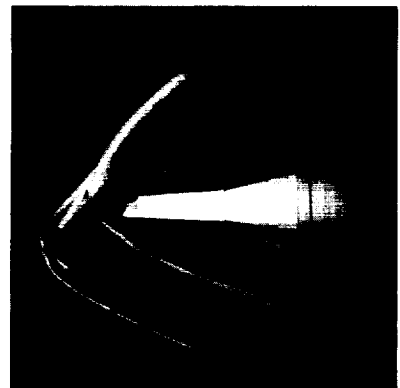
$\alpha = 135^\circ$

$\alpha = 105^\circ$

$\alpha = 150^\circ$

Figure 26.- Schlieren photographs of example airplane configuration indicating change in nature of flow with attitude of the model; $M_\infty = 2.77$.

NASA MEMO 1-17-59A
National Aeronautics and Space Administration.
ESTIMATION OF STATIC LONGITUDINAL STABIL-
ITY OF AIRCRAFT CONFIGURATIONS AT HIGH
MACH NUMBERS AND AT ANGLES OF ATTACK
BETWEEN 0° AND ±180°. Duane W. Dugan.
March 1959. 72p. diagrs., photos.. tab.
(NASA MEMORANDUM 1-17-59A)
(Title, Unclassified)

The possibility of obtaining useful estimates of the
static longitudinal stability of aircraft flying at high
supersonic Mach numbers at angles of attack between
0° and ±180° is explored. Existing theories, empir-
ical formulas, and graphical procedures are employed
to estimate the normal-force and pitching-moment
characteristics of an example airplane configuration
consisting of an ogive-cylinder body, trapezoidal
wing, and cruciform trapezoidal tail.

Copies obtainable from NASA, Washington

1. Flow, Supersonic
          (1.1.2.3)
2. Mach Number Effects -
   Wing Sections (1.2.1.8)
3. Airplanes - Components
   in Combination (1.7.1.1)
4. Missiles - Components
   in Combination (1.7.2.1)
5. Stability, Longitudinal -
   Static   (1.8.1.1.1)
I. Dugan, Duane W.
II. NASA MEMO 1-17-59A

NASA